Edinburgh Research Explorer

Rapid depletion of DIS3, EXOSC10 or XRN2 reveals the immediate impact of exoribonucleolysis on nuclear RNA metabolism and transcriptional control

Rapid depletion of DIS3, EXOSC10 or XRN2 reveals the immediate impact of exoribonucleolysis on nuclear RNA metabolism and transcriptional control

Lee Davidson[1], Laura Francis[#1], Ross A Cordiner[#2,3], Joshua D Eaton[1], Chris Estell[1], Sara Macias[2,4], Javier F Caceres[2] and Steven West[1]*

[1]The Living Systems Institute, University of Exeter, Stocker Rd, Exeter, EX4 4QD, UK

[2]MRC Human Genetics Unit, Institute of Genetics and Molecular Medicine, Western General Hospital, University of Edinburgh, Edinburgh EH4 2XU, UK

[3]Present address: Centre for mRNP Biogenesis and Metabolism, Department of Molecular Biology and Genetics, Aarhus University, C.F. Møllers Alle, Bldg. 1130, 8000 Aarhus C, Denmark

[4]Present address: Institute of Immunology and Infection Research, School of Biological Sciences, University of Edinburgh, Edinburgh, EH9 3FL, UK

[#]Equal contribution

*Lead contact: s.west@exeter.ac.uk. 0044(0)1392 727458

SUMMARY

Cell-based studies of human ribonucleases traditionally rely on methods that deplete proteins slowly. We engineered cells where the $3' \rightarrow 5'$ exoribonucleases of the exosome complex, DIS3 and EXOSC10, can be rapidly eliminated to assess their immediate roles in nuclear RNA biology. Loss of DIS3 has the greatest impact, causing substantial accumulation of thousands of transcripts within 60 minutes. These include: enhancer RNAs, promoter upstream transcripts (PROMPTs) and products of premature cleavage and polyadenylation (PCPA). These transcripts are unaffected by rapid loss of EXOSC10, suggesting that they are rarely targeted to it. More direct detection of EXOSC10-bound transcripts revealed its substrates to prominently include short 3' extended ribosomal and small nucleolar RNAs. Finally, the $5' \rightarrow 3'$ exoribonuclease, XRN2, has little activity on exosome substrates, but its elimination uncovers different mechanisms for early termination of transcription from protein-coding gene promoters.

Keywords: Exosome, EXOSC10/Rrp6, DIS3, Transcription, XRN2, non-coding RNA, Degradation

INTRODUCTION

The RNA exosome is a multi-subunit, 3'→5' exoribonuclease-containing complex originally discovered as important for ribosomal RNA (rRNA) processing (Mitchell et al., 1997). It also plays a crucial role in the turnover of multiple coding and non-coding (nc) transcript classes (Kilchert et al., 2016; Schmid and Jensen, 2018). Many of these transcripts, such as cryptic unstable transcripts (CUTs) in yeast or promoter upstream transcripts/upstream antisense RNAs (PROMPTs/uaRNAs) in humans, are products of antisense transcription (Flynn et al., 2011; Preker et al., 2008; Wyers et al., 2005). An additional class of ncRNA in humans, termed enhancer RNAs (eRNAs), are produced from divergent transcription at intergenic enhancer sequence elements. Like many other pervasive transcripts, eRNAs are highly sensitive to exosome degradation (Andersson et al., 2014). More recently, products of premature cleavage and polyadenylation (PCPA) were also revealed as exosome substrates in mouse embryonic stem cells (Chiu et al., 2018).

The structure of the exosome is similar in yeast and humans and is composed of 9-11 key protein subunits (Gerlach et al., 2018; Januszyk and Lima, 2014; Makino et al., 2013; Weick et al., 2018). It possesses a catalytically inactive barrel structure of 9-core subunits (EXO-9), arranged as a hexamer (the PH-like ring) capped with a trimeric S1/KH ring. EXO-9 interacts with two 3'→5' exoribonucleases: EXOSC10 (Rrp6 in budding yeast) and DIS3 (also known as Rrp44) (Makino et al., 2013). In budding yeast, DIS3 is present in both nuclear and cytoplasmic exosome complexes, but Rrp6 is only found in the nuclear complex (Allmang et al., 1999b). The composition of the exosome is more complicated in humans due to the presence of DIS3 subtypes; however the canonical DIS3 is predominantly found within the nucleoplasm (Tomecki et al., 2010). Similar to Rrp6, EXOSC10 is nuclear and is enriched within the nucleolus (Tomecki et al., 2010). While DIS3 and the core exosome components are essential in budding yeast, cells lacking Rrp6 are viable (Allmang et al., 1999b; Briggs et al., 1998).

EXOSC10 is a member of the RNase D family and contains a DEDD-Y active site providing distributive exoribonuclease activity (Januszyk et al., 2011). DIS3 is a processive ribonuclease related to the RNase II/R family, possessing an RNB and N-terminal PIN domain, and is capable of both exo- and endoribonuclease activity (Lebreton et al., 2008; Schneider et al., 2009). When interacting with the exosome complex Rrp6 is localised on top of the S1/KH cap, close to the entry pore leading into the central channel passing through EXO-9, whereas DIS3 is associated with the channel exit pore at the opposing pole of EXO-9 (Makino et al., 2013; Wasmuth et al., 2014). Rrp6 can widen the entry pore leading into the central channel of EXO-9 facilitating threading of RNAs through EXO-9 towards DIS3 (Wasmuth et al., 2014).

RNA substrates entering the S1/KH cap can also be directed to the active site of Rrp6 for trimming and degradation. Exosome activity is further enhanced by a range of co-factors, including the helicase, MTR4 (Lubas et al., 2011; Weick et al., 2018).

Genome-wide characterisation of human exosome substrates have reported DIS3 as the main ribonuclease subunit responsible for degrading PROMPTs, prematurely terminated protein-coding transcripts and eRNAs (Szczepinska et al., 2015). The targets for EXOSC10 in human cells are less well-characterised, but include rRNA precursors (Macias et al., 2015; Sloan et al., 2013). In budding yeast, the active site of Rrp6 can aid processing of RNA substrates with more complex secondary structures, which is important during maturation of precursor rRNAs (Fromm et al., 2017). The uncovering of previously unknown RNAs has also increased our understanding of transcriptional regulation. For example, the discovery of PROMPTs helped to identify bi-directional transcription from most human promoters (Preker et al., 2008). While our study was in progress, products of PCPA were found to be stabilised by exosome loss, indicating that a proportion of truncated protein-coding RNA precursors are degraded (Chiu et al., 2018). This process is influenced by the recruitment of U1 snRNA to pre-mRNA and may constitute a transcriptional check-point. Both PROMPTs and PCPA products frequently have poly(A) signals (PASs) at their 3' ends and possess poly(A) tails when the exosome is depleted (Almada et al., 2013; Ntini et al., 2013). As such, a PAS-dependent mechanism is proposed for attenuating their transcription.

Studies of the exosome complex in human cells usually involve protein depletion by RNA interference (RNAi), which is slow. Advantages of rapid, versus slower, depletion include reduced opportunities for compensatory effects and an ability to identify the most acute substrates rather than more gradual accumulation of RNA over long time periods, which could be indirect. This is also useful when inferring how frequently a process takes place, which is more difficult when protein depletion is over a period of days. We engineered human cells for rapid, inducible degradation of EXOSC10 or DIS3. Both catalytic components are essential but DIS3 degrades the majority of nuclear exosome substrates. Direct detection of EXOSC10 substrates revealed a role in snoRNAs maturation reminiscent of the situation in budding yeast (Allmang et al., 1999a). Finally, the 5'→3' exonuclease, XRN2, showed little activity on any exosome substrate. However, it promotes early termination of a subclass of transcription events from protein-coding genes suggesting a variety of such mechanisms.

RESULTS

Depletion of EXOSC10 or DIS3 using the auxin-inducible degron system

The auxin-inducible degron (AID) system allows rapid elimination of AID tagged proteins upon addition of auxin to cell culture media (Nishimura et al., 2009). CRISPR/Cas9 was used to C-terminally tag *EXOSC10* or *DIS3* with an AID (Figure 1A). Hygromycin or neomycin resistance markers were incorporated into the cassettes for homology directed repair (HDR) so that bi-allelic modification could be selected for (Eaton et al., 2018). A P2A site, between the AID and drug markers, ensured their separation via peptide cleavage during translation (Kim et al., 2011). This system requires expression of the plant E3 ubiquitin ligase, Tir1, which we previously introduced stably into HCT116 cells - chosen for their diploid karyotype.

Western blotting confirmed successful AID tagging of *EXOSC10* as a species of the predicted molecular weight of EXOSC10-AID was detected in *EXOSC10-AID* cells with native-sized protein absent (Figure 1B). This was confirmed by the exclusive detection of native-sized EXOSC10 in parental *HCT116:TIR1* cells. A time course of auxin addition demonstrated rapid depletion of EXOSC10-AID, which was reduced by ~97% after 60 minutes with native EXOSC10 insensitive to auxin. Western blotting also showed the exclusive presence of DIS3-AID in *DIS3-AID* cells and its depletion upon auxin treatment (Figure 1C). DIS3-AID is expressed at lower levels than native DIS3 and quantitative reverse transcription and PCR (qRT-PCR) showed that there is a ~50% reduction in spliced DIS3-AID mRNA (Figure 1C). A monoclonal antibody to the AID tag also detected DIS3-AID, which is absent from *HCT116:TIR1* cells and eliminated within 60 mins of auxin treatment (Figure 1D). Although DIS3-AID is expressed at lower levels than native DIS3, it does not limit the association of essential co-factors with the exosome core as we observed equal co-immunoprecipitation of EXOSC2 with GFP-MTR4 in *DIS3-AID* and parental cells (Figure 1E).

To demonstrate the specificity of EXOSC10-AID and DIS3-AID depletion, we monitored the levels of several exosome components (EXOSC10, DIS3, EXOSC2, EXOSC3 and MTR4) in parental, *DIS3-AID* and *EXOSC10-AID* cells treated or not with auxin (Figure 1F). Tagging *EXOSC10* or *DIS3* had no impact on the levels of other exosome factors in the absence of auxin. Importantly, auxin treatment specifically eliminated the tagged factors without co-depleting other proteins.

Rapid depletion of EXOSC10-AID or DIS3-AID leads to accumulation of unstable RNAs

We next tested the effects of eliminating EXOSC10-AID or DIS3-AID on some of their known substrates. To check for any adverse effects of auxin addition or the AID tag, we added the parental *HCT116:TIR1* cells to the experimental series. Depletion of EXOSC10 has been shown to stabilise a short 3' extended version of the 5.8S rRNA (Allmang et al., 1999b; Briggs et al., 1998; Schilders et al., 2007). We performed Northern blotting on total RNA isolated from *EXOSC10-AID* cells treated or not with auxin for 60 mins and probed blots for either mature or 3' extended 5.8S rRNA (Figure 2A). 3' extended 5.8S rRNA was weakly detected in treated and untreated *HCT116:TIR1* cells and in untreated *EXOSC10-AID* cells. However, auxin treatment of *EXOSC10-AID* cells induced a strong increase in its levels. As such, acute depletion of EXOSC10 is sufficient to reveal its RNA substrates with no apparent adverse effect of the AID tag.

For DIS3, we analysed the levels of three PROMPTs (STK11IP, SERPINB8, and RBM39) and one anti-sense transcript (FOXP4-AS). This was done in *DIS3-AID* cells treated or not with auxin (60 minutes) and in *HCT116:TIR1* cells grown in the same conditions (Figure 2B). qRT-PCR showed no auxin-dependent changes in *HCT116:TIR1* cells, as expected. PROMPT levels were similarly low in *DIS3-AID* cells untreated with auxin demonstrating that DIS3-AID is sufficient for their normal turnover. However, auxin treatment of *DIS3-AID* cells results in a large increase in all cases confirming the effectiveness of this system.

DIS3 and EXOSC10 are essential in human cells

We next tested whether EXOSC10 and DIS3 are required for cell viability. Colony formation assays were performed on *EXOSC10-AID* or *DIS3-AID* cells grown in the presence and absence of auxin and on *HCT116:TIR1* cells under the same conditions. *HCT116:TIR1* cells formed a similar number of colonies in the presence and absence of auxin demonstrating no adverse effects of auxin on viability (Figure 2C). *DIS3-AID* cells formed as many colonies as *HCT116:TIR1* cells when auxin was omitted, but their smaller size highlights a slight reduction in growth. No *DIS3-AID* cell colonies formed in the presence of auxin showing that DIS3 is essential. *EXOSC10-AID* cells showed no statistically significant defect in colony formation, in the absence of auxin, compared to *HCT116:TIR1* cells (Figure 2D). However, auxin prevented the formation of *EXOSC10-AID* cell colonies showing that EXOSC10 is essential. This contrasts with budding yeast where Δ*rrp6* cells are viable (Allmang et al., 1999b).

Nuclear RNA-seq analysis following EXOSC10-AID or DIS3-AID elimination

We next analysed the immediate impact of EXOSC10 and DIS3 loss more globally. Nuclear RNA was extracted from *EXOSC10-AID* or *DIS3-AID* cells that had been treated, or not, with auxin for one hour and performed RNA-seq. Nuclear RNA was chosen as we anticipated most exosome substrates to be enriched in the nucleus. We first analysed PROMPTs and found an obvious accumulation upon loss of DIS3 (Figure 3A). Importantly, metagene analysis shows that PROMPTs accumulate at thousands of genes when DIS3 is absent (Figure 3B). The global increase in PROMPT levels within just 60 mins of auxin treatment underscores their acute instability. Further examination of the metaplot in Figure 3B revealed no impact of either exosome subunit on the stability of 3' flanking region RNA consistent with our finding that these species are XRN2 substrates (Eaton et al., 2018). Interestingly, acute depletion of EXOSC10 had no effect on PROMPT transcripts suggesting that they are not its immediate substrates.

Hundreds of intergenic transcripts were also seen upon DIS3 elimination, which were barely detectable in the absence of auxin. We presume that these are eRNAs because separating sequencing reads into sense and anti-sense strands showed their bi-directionality (Figure 3C). Moreover, these regions have high H3K4me1 versus H3K4me3 modified chromatin at their promoter regions as do enhancers (Andersson et al., 2014; Core et al., 2014; Heintzman et al., 2007) (Figures S1A and B). Metagene analysis of these transcripts confirmed the generality of the DIS3 effect and, as with PROMPTs, show that they are generally not substrates for EXOSC10 (Figure 3D). Our experiment again highlights the acute instability of eRNAs and straightforward uncovering of almost one thousand examples upon DIS3 loss. This is a similar number to what has reported in other mammalian cells when the exosome was depleted over several days (Pefanis et al., 2015).

Protein-coding promoters also produce a variety of exosome substrates in the sense direction, some of which are generated by PCPA (Chiu et al., 2018; Iasillo et al., 2017; Ogami et al., 2017). Truncated pre-mRNA products are readily apparent in our data following rapid depletion of DIS3 but not when EXOSC10 is lost (Figure 3E). A prominent example is observed for PCF11 pre-mRNA, which is subject to PCPA in mESCs (Chiu et al., 2018). To test the generality of DIS3-mediated turnover of truncated pre-mRNAs we generated a metagene plot covering the first intron of genes (Figure 3F). This showed an obvious enhancement of intron 1 levels in cells depleted of DIS3, with no effect of EXOSC10 loss observed. This effect is still evident when intron read counts are normalised to those over the first exon but, importantly, is diminished over the second or fourth intron (Figures S1C-E). The robust accumulation of such RNAs within minutes of DIS3 loss is an important observation

that underscores the high frequency of attenuated transcription. All of the above DIS3 effects were confirmed in an independent biological RNA-seq replicate (Figure S2).

There is little redundancy between EXOSC10 and DIS3 activity on nucleoplasmic PROMPTs

A striking outcome of our RNA-seq data is the lack of EXOSC10 effect on the thousands of nucleoplasmic exosome substrates degraded by DIS3. In contrast, depletion of EXOSC10 by RNAi often affects nucleoplasmic transcripts and co-depletion of EXOSC10 and DIS3 can produce synergistic effects that imply some redundancy (Lubas et al., 2011; Tomecki et al., 2010). To analyse EXOSC10 effects on nucleoplasmic substrates more closely, we performed a more extended time course of auxin treatment (4 h and 8 h) in *EXOSC10-AID* or *DIS3-AID* cell followed by quantitation of SEPHS1, RBM39 and PPM1G PROMPTs (Figure 4A). Whilst DIS3-AID loss increases the levels of all three transcripts, none were significantly affected by the absence of EXOSC10-AID. Interestingly, MTR4 associates with the exosome core whether or not EXOSC10-AID is present supporting the existence of functional complexes even when EXOSC10 is absent (Figure 4B). We next treated *EXOSC10-AID* cells for 24, 48 or 72 h with auxin, which revealed a mild increase in PROMPTs at longer time points (Figure 4C). As EXOSC10 effects require long-term protein depletion, this could be due to indirect consequences of its loss or reflective of very occasional roles in PROMPT turnover. This is not an indirect effect of auxin as PROMPT levels were unaffected in parental cells after 72 h of treatment (Figure 4D).

The absence of acute EXOSC10 effects on PROMPTs argues that DIS3 degrades them in its absence. To test this, *DIS3-AID* cells were transfected with control or EXOSC10-specific siRNAs before treatment or not with auxin. qRT-PCR was then used to analyse the levels of SEPHS1, RBM39 and PPM1G PROMPTs (Figure 4E). DIS3 elimination from control siRNA treated cells caused upregulation of each PROMPT as expected. For RBM39 this effect was generally not as large as in Figure 2B, which may result from the additional perturbation caused by RNAi. EXOSC10 depletion caused an increase in PROMPT levels even in the presence of DIS3-AID, which is consistent with the small effect of EXOSC10-AID loss at long time-points of auxin treatment. Importantly, auxin treatment of EXOSC10-depleted *DIS3-AID* cells revealed a larger enhancement of PROMPT levels than depletion of either protein alone. As such, although EXOSC10 plays little role in PROMPT RNA degradation under normal circumstances, its presence may be more important when DIS3 levels are very low.

DIS3 loss disrupts focused nucleolar localisation of EXOSC10

To understand why low DIS3 levels may lead to degradation of some nucleoplasmic exosome substrates by EXOSC10 we monitored its localisation in *DIS3-AID* cells treated or not with auxin over a time course (Figure 4F). As previously reported (Lubas et al., 2011; Tomecki et al., 2010), EXOSC10 is nucleolar enriched as shown by co-localisation with nucleolin. Strikingly, DIS3-AID loss resulted in less focussed nucleolar localisation of EXOSC10 (also see Figure S3A). This was not due to a breakdown of nucleoli as nucleolin signal showed little alteration in the same cells. Furthermore, at extended time points of DIS3-AID loss, we observed nucleoplasmic puncta of EXOSC10 in ~25% of cells that do not overlap with nucleolin signal. Importantly, EXOSC10 localisation in *DIS3-AID* cells is identical to the parental cell line and analysis of wider fields of cells confirmed the generality of the effects (Figures S3B-C). We conclude that DIS3-AID loss disrupts the normally focussed nucleolar localisation of EXOSC10, which may allow it to engage with nucleoplasmic substrates and potentially explain the synergistic effect of EXOSC10 and DIS3 co-depletion on PROMPTs.

EXOSC10 is involved in 3' trimming of pre-rRNA and pre-snoRNA transcripts

We next wanted to identify specific substrates of EXOSC10 and utilised individual-nucleotide resolution UV crosslinking and immunoprecipitation (iCLIP) to detect transcripts that it directly binds to. We complemented previous iCLIP data, generated using functional EXOSC10 (EXOSC10^{WT}) in HEK293T cells (Macias et al., 2015), with iCLIP using a catalytically dead version of EXOSC10 (EXOSC10^{CAT}) also expressed in HEK293T cells. EXOSC10^{CAT} contains a single substitution (D313N) previously shown to abolish EXOSC10 activity (Januszyk et al., 2011). We reasoned that EXOSC10^{CAT} would associate more stably with EXOSC10 substrates and facilitate their detection.

As EXOSC10 loss leads to accumulation of 3' extended 5.8S rRNA (Figure 2A), we validated our iCLIP data by first assessing this potential substrate. There was strong iCLIP signal specifically at this site in EXOSC10^{CAT} samples, which had 33 fold more reads mapping within a 30nt window downstream of 5.8S than EXOSC10^{WT} (Figure 5A). This large read density seen in EXOSC10^{CAT} indicates the catalytic mutant is blocking processing of pre-5.8S and underscores it as a *bone fide* EXOSC10 substrate. Consistently, expression of inactive EXOSC10 in *EXOSC10-AID* cells enhances the levels of extended 5.8S RNA in dominant negative fashion (Figures S4A and B). Read density rapidly drops beyond 30nts downstream of the annotated end of 5.8S rRNA, suggesting that EXOSC10 is only required for the final nuclear trimming step. This indicates a ribonuclease switch and is consistent with re-constituted 5.8S rRNA maturation in budding yeast, during which DIS3 processing is sterically inhibited by the exosome core necessitating handover to Rrp6 (Fromm et al., 2017; Makino et

al., 2015). Interestingly, analysis of the entire 45S rDNA showed significant CLIP density over the 5'ETS in both EXOSC10^{WT} and EXOSC10^{CAT} (Figure S4C).

We reasoned that the 30nt "footprint" downstream of the 5.8S rRNA, seen in EXOSC10^{CAT} samples, can identify other RNAs subject to final processing by EXOSC10. Obvious ~30nt footprints of CLIP density were identified in 3' flanking regions of snoRNAs with examples shown for SNORA69 and SNORD18C in Figure 5B. Metagene analyses of the average distribution of EXOSC10 iCLIP reads over annotated snoRNAs indicates that EXOSC10 engages in processing of pre-snoRNAs that are extended at their 3' ends by ~30nts, due to the specific enrichment of CLIP density exclusively seen in the EXOSC10^{CAT} iCLIP dataset (Figure 5C). Indeed, a majority of snoRNAs in both the SNORD and SNORA class showed this signature of EXOSC10^{CAT} binding (Figure S5A). Analysis of our RNA-seq data independently revealed examples where short extended snoRNA precursors are specifically stabilised by EXOSC10 loss (Figure 5D). Overall, these data identify short 3' extended RNA precursors as EXOSC10 substrates. The implication of EXOSC10 in human snoRNA processing highlights conservation with budding yeast where Rrp6 performs a similar 3' trimming step (Allmang et al., 1999a). We also noted examples where longer 3' snoRNA extensions were seen on absence of DIS3 consistent with a ribonuclease handover and previous PAR-CLIP analysis (Szczepinska et al., 2015) (Figure S5B). Finally, unlike for 3' extended snoRNA and 5.8S rRNA, PROMPT and eRNA reads were not enriched in the EXOSC10^{CAT} experiment and the exclusive expression of inactive EXOSC10 did not stabilise PROMPTs (Figures S5C and D). This further demonstrates that they are not usually EXOSC10 substrates.

Analysis of XRN2 regulation of exosome-targeted transcripts

Transcripts can also be degraded from their 5' end with XRN2 being the major nuclear 5'→3' exoribonuclease and having a prominent role in transcriptional termination (Eaton et al., 2018). Although RNAi has also been used to study XRN2, it may not reveal its full repertoire of functions as we suggested previously by engineering *XRN2-AID* cells (Eaton et al., 2018). To more accurately assess the impact of XRN2 on PROMPT and eRNA degradation, we analysed our previously published nuclear RNA-seq from *XRN2-AID* cells in which XRN2 is eliminated within 60 mins of auxin treatment (Figure S6). Interestingly, there was no general impact of XRN2 elimination on either of these transcript classes indicating that they are not its substrates.

The termination of exosome substrates described here is poorly understood, but the *XRN2-AID* cell line allows assessment of its role in the process. Accordingly, we analysed

PROMPT regions in mammalian native elongating transcript sequencing (mNET-seq) data that we previously generated in *XRN2-AID* cells (Eaton et al., 2018). mNET-seq analyses the position of RNA polymerase at single-nucleotide resolution by sequencing the 3' end of RNA from within its active site (Nojima et al., 2015). Comparison of typical PROMPTs (*MYC* and *RBM39*) showed nascent transcription over these regions that terminated within ~1.5kb of the respective promoters (Figure 6A). XRN2 elimination caused neither more reads over the termination region nor additional reads beyond it. More general analysis of the XRN2 impact on PROMPT termination revealed only a very slight increase in signal at the 5'-most positions – also visible in the sense direction (Figure 6B). Therefore, extended PROMPT transcription is not generally apparent in the absence of XRN2. Consistently, RNA-seq revealed no general effect of XRN2 loss on PROMPT levels (Figures S6A and B).

We also show that protein-coding genes produce exosome substrates in the sense direction (Figure 3E and F) and tested the impact of XRN2 on the termination of these products. This analysis was performed on four truncated transcripts at the *PIGV*, *PCF11*, *CLIP4* and *SEPHS1* genes (Figure 3E demonstrates the DIS3 effect for PCF11 and PIGV with CLIP4 and SEPHS1 data in Figure 6C). PCF11 was chosen as it is subject to PCPA in mESCs and has an annotated PCPA site in humans (Ensembl I.D: ENST00000624931.1; Chiu et al., 2018) with the other three genes chosen at random. As truncated transcripts overlap with full-length transcription, we labelled nascent transcripts for 30 mins with 4 thiouridine (4sU) following treatment or not with auxin. 4sU labelled RNA was then captured via biotinylation and streptavidin beads, isolating it from material that pre-existed XRN2 elimination. qRT-PCR was then performed using a primer pair within the DIS3-stabilised region (US) and another downstream of it (DS) (Figure 6D). XRN2 loss induced a significant increase in RNA downstream of the DIS3-stabilised region for PIGV and PCF11, but not for SEPHS1 or CLIP4.

Premature termination may constitute a dead end pathway or it could compete with full-length transcription. To distinguish these possibilities, primers were designed to detect spliced PCF11, PIGV, CLIP4 or SEPHS1 mRNA in 4sU-labelled RNA isolated from *XRN2-AID* cells treated or not with auxin (Figure 6E). Primers were designed to detect spliced RNAs produced by transcription downstream of the attenuated transcript 3' end (~26 kb in the case of PCF11). Interestingly, XRN2 depletion significantly increased the level of spliced mRNA from *PCF11* and *PIGV* suggesting that some transcripts escaping PCPA-mediated termination are not dead-end products. However, spliced SEPHS1 or CLIP4 mRNA were unaffected by XRN2 loss in line with its lack of impact on their attenuated transcription.

Finally, the apparent difference in sensitivity of early termination to XRN2 may be influenced by the frequency of attenuated transcription in each case. To assess this,

attenuated SEPHS1, CLIP4, PIGV and PCF11 transcripts were assayed by qRT-PCR in *DIS3-AID* cells treated or not with auxin (Figure 6F). All four transcripts accumulated robustly on loss of DIS3 demonstrating similarly frequent attenuation of transcription with SEPHS1 showing the largest effect. As such, the insensitivity of SEPHS1 and CLIP4 early termination to XRN2 is not correlated with more infrequent attenuation of transcription compared to PCF11 and PIGV. We conclude that DIS3 is involved in the widespread degradation of attenuated transcripts from protein-coding genes which fall into subtly different classes. We have distinguished some of these on the basis of their sensitivity to XRN2-dependent termination.

DISCUSSION

We have engineered conditional depletion of DIS3, EXOSC10 or XRN2 to assess their immediate impact on RNA metabolism. The rapid depletion achieved provides important insights that complement previous RNAi approaches. Timescales of minutes, versus days, has the obvious advantage that transcripts are less likely to appear through secondary effects. Moreover, an accumulation of RNA within minutes demonstrates constant turnover in a way that is more difficult to infer by RNAi, during which accumulation may be gradual. It also highlights acute substrates versus those that are only apparent after long periods of protein depletion as exemplified by EXOSC10s effect on PROMPT levels.

We were initially concerned that the low levels of DIS3-AID may prove problematic for assaying the impact of its loss. However, several observations mitigate this concern: first, although DIS3 is essential, *DIS3-AID* cells produce as many colonies as *HCT116:TIR1* cells though they are smaller. Second, *DIS3-AID* cells have the same levels of DIS3 substrates as *HCT116:TIR1* cells when auxin is not used. Third, DIS3 substrates do not accumulate upon rapid loss of EXOSC10 activity, underlining the specificity revealed by our approach. Fourth, the level of other exosome components and the integrity of the exosome are not observably different between *DIS3-AID* cells and parental cells.

While PROMPTs are stabilised by RNAi of EXOSC10 from *DIS3-AID* cells, no effect is observed when EXOSC10-AID is rapidly depleted even though *bone fide* substrates are stabilised at this early time-point. Long-term auxin treatment of *EXOSC10-AID* cells does cause a mild increase in PROMPT levels suggesting that RNAi effects are due to prolonged EXOSC10 depletion. This observation suggests that RNAs, such as PROMPTs, are only occasionally targeted by EXOSC10 or that their slight upregulation is an indirect effect of its long-term depletion. A lack of effect of EXOSC10 on PROMPT (and eRNA) turnover is underscored by our iCLIP dataset, which showed that their recovery is not enhanced by inactivating EXOSC10 (Figure S5C). Consistently, PROMPTs are not stabilised even when

EXOSC10 is catalytically inactive (Figure S5D). These experiments demonstrate an evolving impact of EXOSC10 loss on transcript levels over time that may have an indirect explanation that should be considered when interpreting data from long-term depletion.

Our experiments do show some role for EXOSC10 in PROMPT turnover when DIS3 is lost as mis-localisation of EXOSC10 occurs when DIS3-AID is depleted and co-depletion of both proteins synergistically enhances PROMPT levels. Given the nucleolar enrichment of EXOSC10, it may be lacking in a large fraction of nucleoplasmic exosome complexes explaining its limited impact on PROMPTs and other DIS3 substrates. Reciprocally, DIS3 shows relative exclusion from nucleoli, raising the possibility of compartment-specific catalytic complexes (Tomecki et al., 2010). Consistently, we show that EXOSC10 is not required for MTR4 to associate with the exosome core as judged by its continued immunoprecipitation with EXOSC2 in auxin treated *EXOSC10-AID* cells. This is resonant with recent structural data demonstrating MTR4 to contact the human exosome via MPP6 and EXOSC2 and explains how lack of EXOSC10 is compatible with continued degradation of transcripts by DIS3 (Weick et al., 2018).

As it was initially difficult to identify EXOSC10 substrates from our RNA-seq data, we employed iCLIP to detect RNAs directly bound by EXOSC10. This was facilitated by using the inactive protein, which revealed signatures of EXOSC10 binding more robustly than the wild type protein. There was an obvious predominance of short (~30 nts) extended precursors to 5.8S rRNA which we also saw by Northern blotting. The sharp reduction of iCLIP reads beyond this 30nt footprint strongly suggests that EXOSC10 is involved in a final nuclear trimming step similar to what has been shown in budding yeast (Allmang et al., 1999a). Structural studies lend support to this hypothesis having shown that bulky RNA particles can become stalled at the entrance to the central channel of the exosome, necessitating a handover from Rrp44 to Rrp6 (Fromm et al., 2017; Schuller et al., 2018). We suggest that handover is also required for human snoRNA processing because short extended snoRNAs are bound by EXOSC10 and stabilised upon its loss and because previous PAR-CLIP shows DIS3 association with longer snoRNA precursors (Szczepinska et al., 2015). As snoRNAs are often present in introns of expressed genes, stabilised extensions may often be masked by host gene reads in RNA-seq with iCLIP providing a more direct assessment of their fate. We would also like to note that the exosome may act redundantly with other snoRNA processing pathways in humans (Berndt et al., 2012).

In studying the termination of exosome-sensitive RNAs emanating from protein-coding gene promoters, we found that PROMPTs and some truncated sense transcripts are insensitive to XRN2 loss. Even so, many PROMPTs harbour PASs and poly(A) tails and

XRN2 is implicated in some anti-sense transcriptional termination by mNET-seq (Nojima et al., 2015). However, the detection of poly(A) tails does not necessarily mean that polyadenylation occurs on every RNA in a population and it is possible that truncated sense transcripts are generated in multiple ways. Indeed, a complex consisting of the cap-binding complex and ARS2 is implicated in the 3' end processing and termination of short human transcripts including PROMPTs (Hallais et al., 2013; Iasillo et al., 2017). At least some ARS2-sensitive transcripts are generated by mechanisms that do not involve the canonical polyadenylation complex. The differential XRN2 effect on PROMPT and truncated sense transcript termination also suggests a variety of promoter proximal termination processes.

In sum, our data further highlight the constant and rapid turnover of thousands of transcripts in the human nucleus and identify specific substrates for DIS3, EXOSC10 and XRN2. They also reveal that transcripts with apparently similar characteristics (e.g. PROMPTs and PCPA products) can be subtly distinguished on the basis of their sensitivity to XRN2. We anticipate that the ability to rapidly control exoribonucleases, as we have done here, will be especially useful to interrogate processes that cannot be dissected by long term depletion. For example, to test the importance of short-lived RNAs and RNA turnover in stress responses or other changes in cellular environments.

AUTHOR CONTRIBUTIONS

L.D made the *EXOSC10-AID* cell line and derivatives, performed most analysis of it and all bioinformatics. L.F made the *DIS3-AID* cell line and performed most experiments related to it. J.D.E performed all mNET-seq data processing and analysis. C.E performed and analysed the immunofluorescence. R.A.C and S.M performed the EXOSC10 iCLIP, analysed and interpreted the data. J.F.C participated in discussions and writing the manuscript. S.W conceived the project, performed Co-IPs, supervised all experiments (except iCLIP), interpreted results and wrote the paper with input from all authors.

DECLARATION OF INTERESTS

The authors have no competing interests.

STAR METHODS contain the following:

KEY REAGENTS AND RESOURCES TABLE

CONTACT FOR REAGENT AND RESOURCE SHARING

EXPERIMENTAL MODEL AND SUBJECT DETAILS

METHOD DETAILS

- Cell culture and cell lines
- qRT-PCR and 4sU analysis
- Antibodies
- Immunofluoresence
- Nuclear RNA-seq and bioinformatics
- Northern Blot Analysis
- Colony Formation Assay
- iCLIP – Experimental and Computational
- mNET-seq and analysis
- Co-immunoprecipitation
- Primer and DNA sequences

QUANTIFICATION AND STATISTICAL ANALYSIS

DATA AND SOFTWARE AVAILABILITY

REFERENCES

Allmang, C., Kufel, J., Chanfreau, G., Mitchell, P., Petfalski, E., and Tollervey, D. (1999a). Functions of the exosome in rRNA, snoRNA and snRNA synthesis. The EMBO journal *18*, 5399-5410.

Allmang, C., Petfalski, E., Podtelejnikov, A., Mann, M., Tollervey, D., and Mitchell, P. (1999b). The yeast exosome and human PM-Scl are related complexes of 3' --> 5' exonucleases. Genes & development *13*, 2148-2158.

Almada, A.E., Wu, X., Kriz, A.J., Burge, C.B., and Sharp, P.A. (2013). Promoter directionality is controlled by U1 snRNP and polyadenylation signals. Nature *499*, 360-363.

Andersson, R., Refsing Andersen, P., Valen, E., Core, L.J., Bornholdt, J., Boyd, M., Heick Jensen, T., and Sandelin, A. (2014). Nuclear stability and transcriptional directionality separate functionally distinct RNA species. Nat Commun *5*, 5336.

Berndt, H., Harnisch, C., Rammelt, C., Stohr, N., Zirkel, A., Dohm, J.C., Himmelbauer, H., Tavanez, J.P., Huttelmaier, S., and Wahle, E. (2012). Maturation of mammalian H/ACA box snoRNAs: PAPD5-dependent adenylation and PARN-dependent trimming. Rna *18*, 958-972.

Briggs, M.W., Burkard, K.T., and Butler, J.S. (1998). Rrp6p, the yeast homologue of the human PM-Scl 100-kDa autoantigen, is essential for efficient 5.8 S rRNA 3' end formation. J Biol Chem *273*, 13255-13263.

Chen, Y., Pai, A.A., Herudek, J., Lubas, M., Meola, N., Jarvelin, A.I., Andersson, R., Pelechano, V., Steinmetz, L.M., Jensen, T.H.*, et al.* (2016). Principles for RNA metabolism and alternative transcription initiation within closely spaced promoters. Nature genetics *48*, 984-994.

Chiu, A.C., Suzuki, H.I., Wu, X., Mahat, D.B., Kriz, A.J., and Sharp, P.A. (2018). Transcriptional Pause Sites Delineate Stable Nucleosome-Associated Premature Polyadenylation Suppressed by U1 snRNP. Molecular cell *69*, 648-663 e647.

Cong, L., Ran, F.A., Cox, D., Lin, S., Barretto, R., Habib, N., Hsu, P.D., Wu, X., Jiang, W., Marraffini, L.A.*, et al.* (2013). Multiplex genome engineering using CRISPR/Cas systems. Science *339*, 819-823.

Core, L.J., Martins, A.L., Danko, C.G., Waters, C.T., Siepel, A., and Lis, J.T. (2014). Analysis of nascent RNA identifies a unified architecture of initiation regions at mammalian promoters and enhancers. Nature genetics *46*, 1311-1320.

Dodt, M., Roehr, J.T., Ahmed, R., and Dieterich, C. (2012). FLEXBAR-Flexible Barcode and Adapter Processing for Next-Generation Sequencing Platforms. Biology (Basel) *1*, 895-905.

Eaton, J.D., Davidson, L., Bauer, D.L.V., Natsume, T., Kanemaki, M.T., and West, S. (2018). Xrn2 accelerates termination by RNA polymerase II, which is underpinned by CPSF73 activity. Genes & development *32*, 127-139.

Flynn, R.A., Almada, A.E., Zamudio, J.R., and Sharp, P.A. (2011). Antisense RNA polymerase II divergent transcripts are P-TEFb dependent and substrates for the RNA exosome. Proceedings of the National Academy of Sciences of the United States of America *108*, 10460-10465.

Fromm, L., Falk, S., Flemming, D., Schuller, J.M., Thoms, M., Conti, E., and Hurt, E. (2017). Reconstitution of the complete pathway of ITS2 processing at the pre-ribosome. Nat Commun *8*, 1787.

Gerlach, P., Schuller, J.M., Bonneau, F., Basquin, J., Reichelt, P., Falk, S., and Conti, E. (2018). Distinct and evolutionary conserved structural features of the human nuclear exosome complex. Elife *7*.

Hallais, M., Pontvianne, F., Andersen, P.R., Clerici, M., Lener, D., Benbahouche Nel, H., Gostan, T., Vandermoere, F., Robert, M.C., Cusack, S.*, et al.* (2013). CBC-ARS2 stimulates 3'-end maturation of multiple RNA families and favors cap-proximal processing. Nat Struct Mol Biol *20*, 1358-1366.

Heintzman, N.D., Stuart, R.K., Hon, G., Fu, Y., Ching, C.W., Hawkins, R.D., Barrera, L.O., Van Calcar, S., Qu, C., Ching, K.A.*, et al.* (2007). Distinct and predictive chromatin signatures of transcriptional promoters and enhancers in the human genome. Nature genetics *39*, 311-318.

Iasillo, C., Schmid, M., Yahia, Y., Maqbool, M.A., Descostes, N., Karadoulama, E., Bertrand, E., Andrau, J.C., and Jensen, T.H. (2017). ARS2 is a general suppressor of pervasive transcription. Nucleic acids research *45*, 10229-10241.

Januszyk, K., and Lima, C.D. (2014). The eukaryotic RNA exosome. Curr Opin Struct Biol *24*, 132-140.

Januszyk, K., Liu, Q., and Lima, C.D. (2011). Activities of human RRP6 and structure of the human RRP6 catalytic domain. Rna *17*, 1566-1577.

Kilchert, C., Wittmann, S., and Vasiljeva, L. (2016). The regulation and functions of the nuclear RNA exosome complex. Nature reviews Molecular cell biology *17*, 227-239.

Kim, D., Langmead, B., and Salzberg, S.L. (2015). HISAT: a fast spliced aligner with low memory requirements. Nat Methods *12*, 357-360.

Kim, D., Pertea, G., Trapnell, C., Pimentel, H., Kelley, R., and Salzberg, S.L. (2013). TopHat2: accurate alignment of transcriptomes in the presence of insertions, deletions and gene fusions. Genome Biol *14*, R36.

Kim, J.H., Lee, S.R., Li, L.H., Park, H.J., Park, J.H., Lee, K.Y., Kim, M.K., Shin, B.A., and Choi, S.Y. (2011). High cleavage efficiency of a 2A peptide derived from porcine teschovirus-1 in human cell lines, zebrafish and mice. PLoS One *6*, e18556.

Konig, J., Zarnack, K., Rot, G., Curk, T., Kayikci, M., Zupan, B., Turner, D.J., Luscombe, N.M., and Ule, J. (2010). iCLIP reveals the function of hnRNP particles in splicing at individual nucleotide resolution. Nat Struct Mol Biol *17*, 909-915.

Konig, J., Zarnack, K., Rot, G., Curk, T., Kayikci, M., Zupan, B., Turner, D.J., Luscombe, N.M., and Ule, J. (2011). iCLIP--transcriptome-wide mapping of protein-RNA interactions with individual nucleotide resolution. J Vis Exp.

Kopylova, E., Noe, L., and Touzet, H. (2012). SortMeRNA: fast and accurate filtering of ribosomal RNAs in metatranscriptomic data. Bioinformatics *28*, 3211-3217.

Lebreton, A., Tomecki, R., Dziembowski, A., and Seraphin, B. (2008). Endonucleolytic RNA cleavage by a eukaryotic exosome. Nature *456*, 993-996.

Li, H., Handsaker, B., Wysoker, A., Fennell, T., Ruan, J., Homer, N., Marth, G., Abecasis, G., Durbin, R., and Genome Project Data Processing, S. (2009). The Sequence Alignment/Map format and SAMtools. Bioinformatics *25*, 2078-2079.

Liao, Y., Smyth, G.K., and Shi, W. (2013). The Subread aligner: fast, accurate and scalable read mapping by seed-and-vote. Nucleic acids research *41*, e108.

Liao, Y., Smyth, G.K., and Shi, W. (2014). featureCounts: an efficient general purpose program for assigning sequence reads to genomic features. Bioinformatics *30*, 923-930.

Love, M.I., Huber, W., and Anders, S. (2014). Moderated estimation of fold change and dispersion for RNA-seq data with DESeq2. Genome Biol *15*, 550.

Lubas, M., Christensen, M.S., Kristiansen, M.S., Domanski, M., Falkenby, L.G., Lykke-Andersen, S., Andersen, J.S., Dziembowski, A., and Jensen, T.H. (2011). Interaction profiling identifies the human nuclear exosome targeting complex. Molecular cell *43*, 624-637.

Macias, S., Cordiner, R.A., Gautier, P., Plass, M., and Caceres, J.F. (2015). DGCR8 Acts as an Adaptor for the Exosome Complex to Degrade Double-Stranded Structured RNAs. Molecular cell *60*, 873-885.

Makino, D.L., Baumgartner, M., and Conti, E. (2013). Crystal structure of an RNA-bound 11-subunit eukaryotic exosome complex. Nature *495*, 70-75.

Makino, D.L., Schuch, B., Stegmann, E., Baumgartner, M., Basquin, C., and Conti, E. (2015). RNA degradation paths in a 12-subunit nuclear exosome complex. Nature *524*, 54-58.

Mitchell, P., Petfalski, E., Shevchenko, A., Mann, M., and Tollervey, D. (1997). The exosome: a conserved eukaryotic RNA processing complex containing multiple 3'-->5' exoribonucleases. Cell *91*, 457-466.

Nishimura, K., Fukagawa, T., Takisawa, H., Kakimoto, T., and Kanemaki, M. (2009). An auxin-based degron system for the rapid depletion of proteins in nonplant cells. Nat Methods *6*, 917-922.

Nojima, T., Gomes, T., Grosso, A.R.F., Kimura, H., Dye, M.J., Dhir, S., Carmo-Fonseca, M., and Proudfoot, N.J. (2015). Mammalian NET-Seq Reveals Genome-wide Nascent Transcription Coupled to RNA Processing. Cell *161*, 526-540.

Ntini, E., Jarvelin, A.I., Bornholdt, J., Chen, Y., Boyd, M., Jorgensen, M., Andersson, R., Hoof, I., Schein, A., Andersen, P.R.*, et al.* (2013). Polyadenylation site-induced decay of upstream transcripts enforces promoter directionality. Nat Struct Mol Biol *20*, 923-928.

Ogami, K., Richard, P., Chen, Y., Hoque, M., Li, W., Moresco, J.J., Yates, J.R., 3rd, Tian, B., and Manley, J.L. (2017). An Mtr4/ZFC3H1 complex facilitates turnover of unstable nuclear RNAs to prevent their cytoplasmic transport and global translational repression. Genes & development *31*, 1257-1271.

Pefanis, E., Wang, J., Rothschild, G., Lim, J., Kazadi, D., Sun, J., Federation, A., Chao, J., Elliott, O., Liu, Z.P.*, et al.* (2015). RNA exosome-regulated long non-coding RNA transcription controls super-enhancer activity. Cell *161*, 774-789.

Pertea, M., Kim, D., Pertea, G.M., Leek, J.T., and Salzberg, S.L. (2016). Transcript-level expression analysis of RNA-seq experiments with HISAT, StringTie and Ballgown. Nat Protoc *11*, 1650-1667.

Preker, P., Nielsen, J., Kammler, S., Lykke-Andersen, S., Christensen, M.S., Mapendano, C.K., Schierup, M.H., and Jensen, T.H. (2008). RNA exosome depletion reveals transcription upstream of active human promoters. Science *322*, 1851-1854.

Quinlan, A.R., and Hall, I.M. (2010). BEDTools: a flexible suite of utilities for comparing genomic features. Bioinformatics *26*, 841-842.

Ramirez, F., Dundar, F., Diehl, S., Gruning, B.A., and Manke, T. (2014). deepTools: a flexible platform for exploring deep-sequencing data. Nucleic acids research *42*, W187-191.

Schilders, G., van Dijk, E., and Pruijn, G.J. (2007). C1D and hMtr4p associate with the human exosome subunit PM/Scl-100 and are involved in pre-rRNA processing. Nucleic acids research *35*, 2564-2572.

Schmid, M., and Jensen, T.H. (2018). Controlling nuclear RNA levels. Nat Rev Genet *19*, 518-529.

Schneider, C., Leung, E., Brown, J., and Tollervey, D. (2009). The N-terminal PIN domain of the exosome subunit Rrp44 harbors endonuclease activity and tethers Rrp44 to the yeast core exosome. Nucleic acids research *37*, 1127-1140.

Schuller, J.M., Falk, S., Fromm, L., Hurt, E., and Conti, E. (2018). Structure of the nuclear exosome captured on a maturing preribosome. Science *360*, 219-222.

Sloan, K.E., Mattijssen, S., Lebaron, S., Tollervey, D., Pruijn, G.J., and Watkins, N.J. (2013). Both endonucleolytic and exonucleolytic cleavage mediate ITS1 removal during human ribosomal RNA processing. The Journal of cell biology *200*, 577-588.

Szczepinska, T., Kalisiak, K., Tomecki, R., Labno, A., Borowski, L.S., Kulinski, T.M., Adamska, D., Kosinska, J., and Dziembowski, A. (2015). DIS3 shapes the RNA polymerase II transcriptome in humans by degrading a variety of unwanted transcripts. Genome research *25*, 1622-1633.

Tomecki, R., Kristiansen, M.S., Lykke-Andersen, S., Chlebowski, A., Larsen, K.M., Szczesny, R.J., Drazkowska, K., Pastula, A., Andersen, J.S., Stepien, P.P.*, et al.* (2010). The human core exosome interacts with differentially localized processive RNases: hDIS3 and hDIS3L. The EMBO journal *29*, 2342-2357.

Wasmuth, E.V., Januszyk, K., and Lima, C.D. (2014). Structure of an Rrp6-RNA exosome complex bound to poly(A) RNA. Nature *511*, 435-439.

Webb, S., Hector, R.D., Kudla, G., and Granneman, S. (2014). PAR-CLIP data indicate that Nrd1-Nab3-dependent transcription termination regulates expression of hundreds of protein coding genes in yeast. Genome Biol *15*, R8.

Weick, E.M., Puno, M.R., Januszyk, K., Zinder, J.C., DiMattia, M.A., and Lima, C.D. (2018). Helicase-Dependent RNA Decay Illuminated by a Cryo-EM Structure of a Human Nuclear RNA Exosome-MTR4 Complex. Cell *173*, 1663-1677 e1621.

Wyers, F., Rougemaille, M., Badis, G., Rousselle, J.C., Dufour, M.E., Boulay, J., Regnault, B., Devaux, F., Namane, A., Seraphin, B*., et al.* (2005). Cryptic pol II transcripts are degraded by a nuclear quality control pathway involving a new poly(A) polymerase. Cell *121*, 725-737.

Zhang, Y., Liu, T., Meyer, C.A., Eeckhoute, J., Johnson, D.S., Bernstein, B.E., Nusbaum, C., Myers, R.M., Brown, M., Li, W*., et al.* (2008). Model-based analysis of ChIP-Seq (MACS). Genome Biol *9*, R137.

FIGURE LEGENDS

FIGURE 1. Rapid depletion of EXOSC10 or DIS3 via the auxin-inducible degron

(A) Schematic showing the CRISPR strategy for modifying gene loci. Two repair cassettes were generated containing the AID tag, a P2A cleavage site and then either the hygromycin or neomycin resistance marker followed by an SV40 PAS. These were flanked by 5' and 3' homology arms for the gene of interest.

(B) Western blotting of EXOSC10 in either parental Tir1-expressing HCT116 (*HCT116:TIR1*) or *EXOSC10-AID* cells. A time course of auxin addition was applied to the *EXOSC10-AID* cells. Equal loading is shown by the presence of a non-specific product (*) on the same blot.

(C) Western blotting of DIS3 in either *HCT116:TIR1* or *DIS3-AID* cells treated or not for 60 minutes with auxin. Tubulin was probed for as a loading control. qRT-PCR-derived levels of DIS3 mRNA also shown (including standard deviation) obtained following normalisation to GAPDH levels.

(D) Western blotting of DIS3 in either *HCT116:TIR1* or *DIS3-AID* cells treated or not for 60 minutes with auxin using an antibody to the AID tag. Tubulin was probed for as a loading control.

(E) Co-immunoprecipitation (Co-IP) of GFP-MTR4 and EXOSC2 in *HCT116:TIR1* or *DIS3-AID* cells. Input (5%) and IP are shown. Blots were probed with α-GFP (to detect GFP-MTR4) or α-EXOSC2.

(F) Western blotting of EXOSC10, DIS3, MTR4, EXOSC2, EXOSC3 and, as loading control, CPSF73 in *HCT116:TRI1*, *DIS3-AID* or *EXOSC10-AID* cells treated or not with auxin (1h).

Due to the similar size of some of these proteins, multiple blots were probed rather than employing stripping. Equal loading was confirmed by loading control/ponceau. Pictures of individual blots are deposited at Mendeley (see methods).

FIGURE 2. Effects of DIS3/EXOSC10 depletion on RNA substrates and cell viability

(A) Northern blot analysis of mature (lower panel) and 3' extended (upper panel) 5.8S rRNA performed in *HCT116:TIR1* cells and *EXOSC10-AID* cells treated or not with auxin. Bar graph shows quantitation expressed as a ratio of extended to mature species. n=3. * denotes p<0.05. Error bars are standard deviation.

(B) qRT-PCR detection of STK11IP, SERPINB8, FOXP4-AS and RBM39 PROMPTs in *HCT116:TIR1* cells and *DIS3-AID* cells treated or not with auxin (1h). Quantitation is expressed as relative RNA level relative to that found in non-auxin treated *HCT116:TIR1* cells after normalising to ACTB RNA. n=3. * denotes p<0.05. Error bars are standard deviation.

(C) Colony formation assay for HCT116:TIR1 cells and *DIS3-AID* cells grown with or without auxin. Number of colonies expressed as a percentage of those forming from *HCT116:TIR1* cells grown in the absence of auxin. Values show average and standard deviation from n=3.

(D) As for (C) but for *HCT116:TIR1* and *EXOSC10-AID* cells.

FIGURE 3. Global analysis of the effects of EXOSC10 or DIS3 loss

(A) Integrative genome viewer (IGV) browser tracks of MARS2, PPM1G and SEPHS1 PROMPT transcripts (boxed) in *EXOSC10-AID* and *DIS3-AID* cells treated or not with auxin. Y-axis units are reads per kilobase per million mapped (RPKM).

(B) Metagene plot of coding and non-coding genes in *EXOSC10-AID* and *DIS3-AID* cells treated or not with auxin. DIS3 loss shows a strong effect on PROMPT regions (boxed).

(C) IGV browser tracks of two eRNA regions in *EXOSC10-AID* and *DIS3-AID* cells treated or not with auxin. Y-axis units are RPKM.

(D) Metagene plot of all eRNA expressing regions in *EXOSC10-AID* and *DIS3-AID* cells treated or not with auxin.

(E) IGV browser tracks of *PCF11* and *PIGV* in *EXOSC10-AID* and *DIS3-AID* cells treated or not with auxin. Both show strong upregulation of 5' pre-mRNA upon loss of DIS3 (boxed). Y-axis units are RPKM.

(F) Metagene plot of all first introns in *EXOSC10-AID* and *DIS3-AID* cells treated or not with auxin.

FIGURE 4. Analysis of redundancy between EXOSC10 and DIS3

(A) qRT-PCR analysis of PPM1G, SEPHS1 and RBM39 PROMPTs in *DIS3-AID* or *EXOSC10-AID* cells treated or not with auxin for 4 and 8 h. Levels are expressed as fold change compared to untreated cells (indicated by dotted line) following normalisation to GAPDH mRNA. n=3. * denotes p<0.05 for differences concluded on in the text. Error bars show standard deviation.

(B) Co-immunoprecipitation of EXOSC10 or EXOSC2 with GFP-MTR4 in *EXOSC10-AID* cells treated or not with auxin (2 h). Input and IP are shown with blots probed with α-GFP (to detect GFP-MTR4), α-EXOSC10 or α-EXOSC2.

(C) qRT-PCR analysis of PPM1G, SEPHS1 and RBM39 PROMPTs in *EXOSC10-AID* cells treated or not with auxin for 24, 48 or 72h. Levels are expressed as fold change compared to untreated cells (indicated by dotted line) following normalisation to GAPDH mRNA. n=3. * denotes p<0.05 for differences concluded on in the text. Error bars show standard deviation.

(D) qRT-PCR analysis of PPM1G, SEPHS1 and RBM39 PROMPTs in *HCT116:TIR1* cells treated or not with auxin for 72h. Levels are expressed as fold change compared to untreated cells (indicated by dotted line) following normalisation to GAPDH mRNA. n=3. Error bars show standard deviation.

(E) qRT-PCR analysis of PPM1G, SEPHS1 and RBM39 PROMPTs in *DIS3-AID* cells transfected with control or EXOSC10-specific siRNAs before treatment, or not, with auxin (1h). Levels are expressed as fold change compared to control siRNA transfected cells untreated with auxin following normalisation to GAPDH mRNA. n=4. * denotes p<0.05 for differences concluded on in the text. Error bars show standard deviation.

(F) EXOSC10 immunofluorescence in untreated *DIS3-AID* cells or the same cells treated with auxin for 1, 2, 3 or 4 h. The same cells stained with nucleolin are also shown. The red arrows show EXOSC10 puncta that do not overlap with nucleolin signal.

FIGURE 5. Direct detection of EXOSC10 substrates by iCLIP

(A) iCLIP trace of 5.8S rRNA locus obtained from EXOSC10[WT] and EXOSC10[CAT] samples. There is a clear enrichment of reads for the EXOSC10[CAT] sample showing a 30 nucleotide

"footprint" immediately beyond the 5.8S gene (indicated by vertical lines). Y-axis units are reads per million mapped.

(B) iCLIP traces of *SNORA69* and *SNORD18C* genes obtained from EXOSC10^{WT} and EXOSC10^{CAT} samples. There is strong enrichment of reads for the EXOSC10^{CAT} sample showing a 30 nucleotide "footprint" immediately beyond each gene. Y-axis units are reads per million mapped.

(C) Metagene plots of iCLIP reads over the 5' or 3' regions of snoRNA genes in EXOSC10^{WT} and EXOSC10^{CAT} samples. There is a clear 30 nucleotide "footprint" immediately 3' of snoRNA genes.

(D) IGV browser tracks of *SNORA48* and *SNORA68* genes in *EXOSC10-AID* and *DIS3-AID* cells treated or not with auxin. These show upregulation of short 3' extended versions of each (boxed) in auxin-treated *EXOSC10-AID* cells. Y-axis units are RPKM.

FIGURE 6. Effects of rapid XRN2 loss on exosome substrates and early transcriptional termination

(A) *MYC* and *RBM39* PROMPT region tracks in mNET-seq data obtained from *XRN2-AID* cells treated or not with auxin. y-axes show signals per 10^8 mapped reads.

(B) Metagene analysis of PROMPT regions (boxed) in mNET-seq data obtained from *XRN2-AID* cells treated or not with auxin. TPM denotes transcripts per million. Signal below zero on the y-axis represents antisense PROMPT transcription.

(C) Gene tracks of *CLIP4* and *SEPHS1* attenuated transcription in *EXOSC10-AID* or *DIS3-AID* cells treated or not with auxin (1 hr). Truncated RNAs stabilised by DIS3 loss are boxed. Y-axis shows RPKM.

(D) qRT-PCR analysis of premature transcriptional termination at *PCF11, PIGV, CLIP4* and *SEPHS1* genes in 4sU-labeled RNA from *XRN2-AID* cells treated or not with auxin (1h). A gene track for *PCF11* shows DIS3-stabilised products together with approximate primer positions. Red arrow denotes annotated PCF11 PCPA product. The same primer position principles apply to the other three genes tested. Graph shows quantitation where values are plotted relative to those in untreated *XRN2-AID* cells following normalisation to spliced GAPDH mRNA levels. n≥3. * denotes p<0.05. Error bars show standard deviation.

(E) qRT-PCR analysis of spliced PCF11, PIGV, CLIP4 and SEPHS1 mRNA in 4sU-labeled RNA extracted from *XRN2-AID* cells treated or not with auxin (1h). Graph shows quantitation

where values are plotted relative to those in untreated *XRN2-AID* cells following normalisation to spliced GAPDH mRNA levels. n≥3. * denotes p<0.05. Error bars show standard deviation.

(F) qRT-PCR quantitation of the DIS3 effect on truncated PCF11, PIGV, CLIP4 and SEPHS1 transcripts determined in *DIS3-AID* cells treated or not with auxin (1h). Graph shows quantitation where values are plotted relative to those in untreated *DIS3-AID* cells following normalisation to spliced GAPDH mRNA levels. n≥3. Error bars show standard deviation.

STAR METHODS

KEY REAGENTS AND RESOURCES TABLE

REAGENT or RESOURCE	SOURCE	IDENTIFIER
Antibodies		
AID	MBL	Cat# M214-3
EXOSC10 (Fig1 B)	abcam	Cat# Ab50558
EXOSC10 (other figures)	Santa Cruz	Cat# Sc-374595-X
DIS3	Bethyl DIS3	Cat# A303-765A
Nucleolin	abcam	Cat# Ab22758
MTR4	Bethyl	Cat# A300-614A
GFP	abcam	Cat# ab290
EXOSC3	abcam	Cat# ab156683
MYC	Santa Cruz	Cat# sc-40
Mouse Alexa Flour 555	Invitrogen	Cat# A-21424
Rabbit Alexa Fluor 488	Invitrogen	Cat# A-11034
CPSF73	abcam	Cat# ab131245
EXOSC2	abcam	Cat# ab181211
Tubulin	abcam	Cat# ab7291
Anti-FLAG® M2 Magnetic Beads	Sigma	Cat# M8823-1ML
Chemicals, Peptides, and Recombinant Proteins		
Auxin	Sigma	Cat# I3750-5G-A
Benzonase	Sigma	Cat# E1014-5KU
Critical Commercial Assays		
Plasmid mini-prep kit	Qiagen	Cat# 27106
Gibson assembly mastermix (for cloning)	NEB	Cat# E5510S
GFP-Trap beads	Chromotek	Cat# Gtma-20
QuikChange II XL Site-Directed Mutagenesis Kit	Stratagene	Cat# 200521
QIAquick nucleotide removal kit	Qiagen	Cat# 28304
Deposited Data		
Sequencing data EXOSC10 and DIS3	Gene Expression Omnibus	GSE120574
Sequencing data XRN2	Gene Expression Omnibus	GSE109003
Uncropped blots	Mendeley	https://data.mendeley.com/datasets/jyh2wdyb7z

EXOSC10 WT iCLIP Biological replicate 1 & 2	(Macias et al., 2015); Gene Expression Omnibus	GSM1892061 & GSM1892062
EXOSC10 CAT iCLIP data	Gene Expression Omnibus	GSE120574
H3K27ac ChIP-seq	Gene Expression Omnibus	GSE31755
H3K4me1 ChIP-seq	Gene Expression Omnibus	GSE31755
H3K4me3 ChIP-seq	Gene Expression Omnibus	GSE35583
ChIP input control	Gene Expression Omnibus	GSE31755
Experimental Models: Cell Lines		
HCT116:TIR1	(Eaton et al., 2018)	N/A
DI3-AID	This paper	N/A
EXOSC10-AID	This paper	N/A
XRN2-AID	(Eaton et al., 2018)	N/A
EXOSC10-AID + EXOSC10 CAT	This paper	N/A
EXOSC10-AID + EXOSC10 WT	This paper	N/A
Oligonucleotides		
Control siRNA	Thermofisher	Cat# AM4613
EXOSC10 siRNA	Thermofisher	Silencer select: S10738
qPCR primers	This paper	Supplemental material
iCLIP Oligo: L3 3' RNA adapter: 5'Phosphate-UGAGAUCGGAAGAGCGGUUCAG-3'Puromycin	(Konig et al., 2010)	N/A
iCLIP Oligo: rtCLIP_5: 5'Phosphate-NNCGCCNNNAGATCGGAAGAGCGTCGTGgatcCTGAACCGC	(Konig et al., 2011)	N/A
iCLIP Oligo: Cut_oligo: GTTCAGGATCCACGACGCTCTTCaaaa	(Konig et al., 2011)	N/A
iCLIP Oligo: P5Solexa : AATGATACGGCGACCACCGAGATCTACACTCTTTCCCTACACGACGCTCTTCCGATCT	(Konig et al., 2011)	N/A
iCLIP Oligo: P3Solexa : CAAGCAGAAGACGGCATACGAGATCGGTCTCGGCATTCCTGCTGAACCGCTCTTCCGATC	(Konig et al., 2011)	N/A
5.8S Northern probe: GCAAGTGCGTTCGAAGTGT	This paper	N/A
5.8S 3' EXT Northern probe: GGGGCGATTGATCGGCAA	This paper	N/A
Primer pairs for qRT-PCR	This paper	Table S1
Recombinant DNA		
px330 for CRISPR	(Cong et al., 2013)	Addgene Cat# 42230
GFP-MTR4	(Lubas et al., 2011) A kind gift from the lab of Torben Jensen	N/A
Plasmids for DIS3 tagging	This paper	Critical sequences in Supplemental material
Plasmids for EXOSC10 tagging	This paper	Critical sequences in supplemental material
EXOSC10WT for iCLIP	This paper and (Macias et al., 2015)	N/A

EXOSC10CAT for iCLIP	This paper	N/A
EXOSC10WT for Figures S4A, 7B,	This paper	N/A
EXOSC10CAT for Figures S4A, 7B	This paper	N/A
Software and Algorithms		
pyCRAC	(Webb et al., 2014)	N/A
TopHat2	(Kim et al., 2013)	N/A
BEDTools	(Quinlan and Hall, 2010)	N/A
Image J (colony counting and image processing)		N/A
MACS2	(Zhang et al., 2008)	N/A
deeptools	(Ramirez et al., 2014)	N/A
featureCounts	(Liao et al., 2014)	N/A
DESeq2	(Love et al., 2014)	N/A
StringTie	(Pertea et al., 2016)	N/A
SortMeRNA	(Kopylova et al., 2012)	N/A
HISAT2	(Kim et al., 2015)	N/A
SAMTools	(Li et al., 2009)	http://samtools.sourceforge.net/
Other		
eRNA & PROMPT annotations	(Chen et al., 2016)	N/A

CONTACT FOR REAGENT AND RESOURCE SHARING

Further information and requests for resources and reagents should be directed to and will be fulfilled by the Lead Contact, Steven West (s.west@exeter.ac.uk).

EXPERIMENTAL MODEL AND SUBJECT DETAILS

Experiments involved human colon carcinoma derived HCT116 cells (male) and human embryonic kidney derived HEK293T cells (female).

METHOD DETAILS

Cell culture and cell lines

HCT116 and HEK293T were cultured in Dulbecco modified eagle medium with 10% foetal calf serum. Our CRISPR protocol and plasmids was described previously (Eaton et al., 2018). Sequences of EXOSC10 and DIS3 homology arms are provided in this manuscript. Briefly, HCT116 cells grown on a 30mm dish were transfected with 1ug each of guide RNA plasmid, Neomycin and Hygromycin repair constructs. Transfection was with Jetprime (Polyplus) following the manufacturers' guidelines. Media was changed after 24 hours and, after 72 hours, cells were re-plated into 100mm dishes in media containing 30ug/ml Hygromycin and 800ug/ml Neomycin. Resistant colonies were picked and screened by PCR 10-14 days later. Correct genomic insertion of tags was assayed by sequencing these PCR products. Auxin was used at a concentration of 500uM for one hour unless stated otherwise. For RNAi, 24-well dishes were transfected with siRNA using Lipofectamine RNAiMax (Life

Technologies) following the manufacturers' guidelines. The transfection was repeated 24 hours later and, 72 hours after the first transfection, RNA was isolated.

qRT-PCR and 4sU analysis

In general 1ug of RNA was isolated using Tri-reagent and DNAse treated for one hour before reverse transcription (Protoscript II) using random hexamers. cDNA products were diluted to 50ul volumes. 1ul was used for real-time PCR in a Qiagen Rotorgene instrument using Brilliant III SYBR mix (Agilent technologies). The comparative quantitation option in the software was used to generate graphs. The 4sU qRT-PCR protocol is as described in Eaton *et al* 2018.

Immunofluoresence

Cells were grown on cover slips, treated for 0, 1, 2, 3, or 4 hours with auxin, washed with PBS, fixed for 10 minutes in 4 % PFA, washed with PBS, permeabilised with 0.1 % Triton x-100 (*v/v* in PBS) for 10 minutes, then blocked with 10 % FBS (*v/v* in PBS) for 1 Hour. Cells were probed overnight with 1:1000 diluted α-EXOSC10 and α-nucleolin at 4 °C, washed with 0.01 % NP40 (*v/v* in PBS), probed with Alexa Fluor® 488 anti-rabbit and Alexa Fluor® 555 anti-mouse secondary's (1:2000, Invitrogen) for 1 hour, counter stained with DAPI, washed and mounted. All images were taken using an Olympus-81 oil immersion microscope, exposure times, brightness and contrast settings are identical between images.

Nuclear RNA-seq

Nuclei were extracted using hypotonic lysis buffer (10 mM Tris pH5.5, 10 mM NaCl, 2.5 mM $MgCl_2$, 0.5% NP40) with a 10% sucrose cushion and RNA was isolated using Tri-reagent. Following DNase treatment, RNA was Phenol Chloroform extracted and ethanol precipitated. After assaying quality control using a Tapestation (Agilent), 1 μg RNA was rRNA-depleted using Ribo-Zero Gold rRNA removal kit (Illumina) then cleaned and purified using RNAClean XP Beads (Beckman Coulter). Libraries were prepared using TruSeq Stranded Total RNA Library Prep Kit (Illumina) and purified using Ampure XP beads (Beckman Coulter). A final Tapestation D100 screen was used to determine cDNA fragment size and concentration before pooling and sequencing using Hiseq2500 (Illumina) at The University of Exeter sequencing service. GEO accession numbers: (*EXOSC10-AID* and *DIS3-AID* cell RNA-seq: GSE120574), (*XRN2-AID* cell RNA-seq: GSE109003).

RNA-Seq Read Alignment

Raw single-end 50bp reads were screened for sequencing quality using FastQC; adapter sequences were removed using Trim Galore! and trimmed reads shorter than 20 bp were discarded. All nuclear RNA-seq analyses were carried out using the Ensembl GRCh38.p10 and GRCh38.90 human gene annotations. Before alignment, trimmed reads were passed through the SortMeRNA pipeline (Kopylova et al., 2012) to remove trace rRNA matching in-built 18S and 28S human databases then mapped to GRCh38 using HISAT2 (Kim et al., 2015) with default parameters supplemented with known splice sites. Unmapped, multimapped and low MAPQ reads (< 20) were discarded from the final alignment using SAMtools (Li et al., 2009).

de novo Transcript Assembly

de novo transcripts were assembled from each library using the StringTie suite (Pertea et al., 2016) with default parameters, guided by current GRCh38 reference annotation. Known annotated genes were dropped and the assembled transcripts from each sample were merged into a single consensus annotation. Reads were then counted per transcript using featureCounts (Liao et al., 2013, 2014) and differentially expressed upregulated de novo gene intervals (≥ 2-fold, padj < 0.05) were called using DESeq2 (Love et al., 2014). de novo transcripts were designated as a PROMPT (<3 kb) or eRNA (> 3 kb) based on their relative distance from the nearest annotated gene.

Generation of Synthetic Intron Annotation

A custom intron annotation file was produced from GRCh38 by merging all exon intervals derived from each transcript isoform to generate a synthetic transcript representative of every gene. Each synthetic exon was then subtracted from gene intervals using the BEDtools suite (Quinlan and Hall, 2010) producing intron intervals with inherited gene information. Synthetic introns were counted and numbered according to their strand orientation i.e. sense introns numbered ascending, antisense introns descending, finally merging into a single annotation file.

Meta Profiling

PROMPT and eRNA Analysis

For metagene analysis, expressed protein-coding and ncRNA genes (> 50 reads per gene) were selected and an extended transcriptional window was then applied to each gene to include a 3 kb region 5' of the TSS and a 7 kb region 3' of the TES. Overlapping genes and genes that extended beyond chromosome ends were discarded using the BEDtools suite to prevent double read counting. Profiles of these filtered genes were then generated from RPKM normalised reads using deeptools (Ramirez et al., 2014) with further graphical processing performed in the R environment (http://www.R-project.org). Normalised coverage plots (RPKM) were visualised using the Integrative Genome Viewer (IGV) suite. For eRNA meta profiles, no extended window was applied and plots were generated directly from RPKM normalised reads and the *de novo* eRNA annotation file.

Peak Calling from ChIP-seq Analysis

ChIP-Seq data was generated by ENCODE from immunoprecipitation (IP) of acetylated histone 3 lysine 27 (H3K27ac) (GEO: GSE31755), monomethylated histone 3 lysine 4 (H3K4me1) (GEO: GSE31755), trimethylated histone 3 lysine 4 (H3K4me3) (GEO: GSE35583) and an input control sample (GEO: GSE31755) in unmodified HCT116 cells. Raw single-end ChIP-seq reads were processed to remove adapter sequences and low quality reads then mapped to GRCh38 using spliced alignment disabled HISAT2 parameters. BAM alignment files were converted to BED and duplicate reads were discarded and collapsed into a coverage BEDGRAPH file. Peaks were called using MACS2 (Zhang et al., 2008). A background ChIP-Seq signal calculated from the input control sample was compared against each histone modification after sequencing depth normalisation, generating a set of peaks for each mark. Peaks were then passed through a Poisson test to call peaks with a qvalue cut-off < 0.05 producing coverage files of peak enrichment. Enrichment of H3K4me1 and H3K4me3 marks were compared and visualised as a log2 ratio using deeptools.

Northern Blot Analysis

Total RNA was separated on a 12% Urea-PAGE gel, transferred on to a Hybond-N+ nylon membrane (GE Healthcare), dried and UV crosslinked (2 x 1200 µjoules/cm2) before blocking in hybridisation buffer (6x SSPE [150 mM NaCl, 9 mM NaH_2PO_4, 1 mM EDTA (pH to 7.4], 5x Denhardt's Reagent, 0.2% SDS) at 37°C for 1 hour. DNA probes were 5' radiolabelled with [γ-^{32}P]ATP using T4 PNK (NEB) and cleaned with Qiagen QIAquick nucleotide removal kit. Probes were then added to the hybridisation buffer and incubated at 42°C overnight. Membranes were then rinsed in hybridisation buffer 3 times for 1 minute then washed at 42°C

for 15 minutes before drying and developing on a Phosphor screen. Images were developed on a GE Typhoon FLA 7000 (GE Healthcare). Developed images were then quantitated and analysed using the ImageJ suite. Membranes were probed with the 5.8S 3' ext probe first before stripping and re-probing with the mature 5.8S probe.

Colony Formation Assay

Cells were seeded into 100 mm cell culture plates and grown in auxin or ethanol (solvent) for 10 days. Growth media and auxin were replaced every 2-3 days. Colonies were fixed in ice cold methanol for 10 minutes and stained using 0.5% (w/v) crystal violet + 25% (v/v) methanol for 10 minutes. Stained colonies were counted using the ImageJ particle analyser function. Genuine colonies were defined as existing at a density ranging between 50-8000 pixels with a circularity rating between 0.75-1 (1 = perfect circle).

iCLIP - Experimental

3xFLAG-EXOSC10^{CAT} was generated from 3xFLAG-EXOSC10^{WT} using Quick-change site-directed mutagenesis kit (Stratagene) to introduce a single amino acid change from Aspartic acid to Asparagine (D313N) within the conserved DEDD-Y motif rendering EXOSC10 catalytically inactive. HEK293T cells were seeded into 15cm plates and transiently transfected with 3xFLAG-EXOSC10^{CAT} and collected 48hrs later when 90% cell confluency was reached. Cells were crosslinked twice on ice using 120 mJ/cm^2 UVC irradiation, with ice cold PBS replaced after each cross-linking phase. iCLIP was performed on these cell pellets based on the protocol outlined in (Konig et al., 2011). FLAG-tagged proteins were purified using M2 FLAG Dynabeads. A RNA linker (5′Phosphate-UGAGAUCGGAAGAGCGGTTCAG-3′Puromycin) was ligated to the 3′ end of RNAs, which was described in Konig et al (Konig et al., 2010). Libraries were sequenced using the Illumina HiSeq system (Bejing Genomics Institute).

iCLIP - Computational

Reads were demultiplexed, processed and PCR duplicates were collapsed using Flexbar (Dodt et al., 2012), FASTX-Toolkit (http://hannonlab.cshl.edu/fastx_toolkit/), and custom perl scripts, respectively. Biological replicates were combined to increase coverage. Reads were mapped to either Hg38 or a consensus sequence for 45S rDNA using Tophat with the --max-multihits 1 option called. Genome browser files were normalised to reads per

million mapped. Average distribution plots for snoRNAs were generated using pyReadCounters.py and pyBinCollector.py from the pyCRAC software package (Webb et al., 2014). iCLIP data for 3xFLAG-EXOSC10^{WT} was obtained from (Macias et al., 2015; GSM1892061 and GSM1892062) and analysed in parallel with EXOSC10^{CAT} data (GSE120574). SnoRNA table was generated by identifying any snoRNA that had an EXOSC10 iCLIP read mapped within 50nt downstream of the 3' end of a mature snoRNA. PROMPT and eRNA annotations were derived from (Chen et al., 2016).

mNET-seq

The mNET-seq experiment and analyses pipeline are as previously published in (Eaton et al., 2018). The XRN2-AID data are deposited with Gene Expression Omnibus (GSE109003).

Co-immunoprecipitation

Approximately 5 million cells were transfected with 5µg of GFP-MTR4 plasmid and the following day, lysed in IP lysis buffer (150mM NaCl, 2.5mM MgCl$_2$, 20mM Tris.HCl pH7.5, 1% Triton X-100) by incubation on ice for 30 mins with 1µl of Benzonase. Lysates were clarified by centrifugation (12000rpm for 10 mins) and then incubated with 20µl GFP-TRAP beads (Chromotek) for 1 hour at 4°C with rotation. Beads were washed four times with IP lysis buffer and complexes eluted in 2x SDS gel loading buffer for analysis by western blotting.

EXOSC10 HDR 5'

TTGATCCTCCCGCCTTGGCCTCCCAGAGTACTGGGATTACAGGTGTGAGCCACTGCAC
CCAGCCAAATGTTTTTGTTAAAAACATAAAATCCTAATAATTAAGCCGACCCTGAGGTCA
GGGGACTTGCCCGAGGGCAGGAAAAACAGGTCTGCCTTCTCAAGATGCTGCTCAGCTC
AGCCAACTCTGGTGGGCCGCCGAGTTCTCTGGGGCCCCTGAGCAAACCATTCTTCCTC
TGTTCTGCATGATTAAGATTTGCACCATTTTGTAAACCATCTGAGAACATCCAACCAGCC
CGGAAGAAATAACTGTTGTTTTTGTACTCTCTGCAGAGGCTTCAGGTACAACTGGCCAC
AGAGA

EXOSC10 HDR 3'

TAGTCCTGGAAGACACGTGGCGCCTGTGGACCGGAAGCACCAAATGCTGGTGCTGCTT
TTGTACATACATATTTTTAAACCATTAAAATTCTTCCTGAAGAAAGCTGATTCCTGACTTT

TATTTTGTTGCCGCCACAGCTCTGGCAGGTTGCCATCCTGTTCAGGCAACCATCTTCAG
CTGTCTGTGGGCAGGTGAGTGTGCTCCGGGGGTTATGGTGACTTCTAGAAAAATCCAG
AGCCGGCCGGGTGCGGTGGCTCACGCCTGCAATCCCAGCACTTTGGGAGGCTGAGGC
AGGCGGATCACGAGGTCAGGAGATCGAGACCATGCTGGCCAACACGGTGAAAGC

EXOSC10 gRNA target: AGATAGTCCTGGAAGACACG

DIS3 HDR 5'

CTTGAAATCAACTCTGATTCTGTCAATCACAGTGGCTCCCCATTGGGAAGGCTGTTTTG
TAGTTAAAAAGAACACTTCCTAAATGACATGCTTCTCACCTGTTGAGACCATGTCTAGCT
TTTACATTTTTGAACCACTGCTACTTTGTAAATACCTTCTGTGTATAAAACCTTTAATTA
GCCCCCTTTCCCCTCCCTACCACTACATCCTTTTAAATTTGAAGCTGGCAGTGGGGAAG
GGGAGGATGAGGTTGAGATGTATTCTATCCTTTAAATCACCTTATTTCCCCCCATTTGCA
TTACTTTAGATACCAGGAATAAGCATTCCTACAGACACATCTAACATGGACCTTAATGGA
CCAAAGAAAAAGAAGATGAAGCTTGGAAAA

DIS3 HDR 3'

TAGCTATATTCAACAAAAATCTTCAAAGACTGGTTTCTTTTTTAAAAGAAAAAACTTGAAA
GAACACTTCTAAGCCTAAGTGTGTGATACAGTTTGTTACTTTTAAGTACATTTTAATAATT
TCAGACATCTGCATTTTTATTGAACAGTTGACTGTATCTGACCCATCATACTACTATACTT
CTGGGTTGAACAGAATTATTTATGCAGAATAATTCAATTGAATATCCATCACTTAAATACA
GTGACAGGACAGCAACTTCAGGGATCTGTAAAGATCATTTAAATGGAGT

DIS3 gRNA target: ACTGATACTTCAAACATGGA

Codon optimised *IAA17* (AID)

GGTAGTGGCATGATGGGTAGTGTGGAGCTGAACCTGCGCGAGACCGAGCTGTGCTTG
GGACTGCCTGGCGGCGATACGGTTGCACCCGTTACCGGGAACAAGAGGGGCTTCAGC
GAGACAGTGGATCTCAAGCTGAATCTGAACAACGAACCTGCAAATAAAGAGGGAAGCA
CCACTCATGACGTAGTGACATTCGATAGTAAAGAGAAATCTGCTTGCCCGAAGGATCCA
GCTAAGCCCCCGGCCAAGGCCCAGGTGGTGGGATGGCCCCCGGTGCGCTCCTACCG
CAAAAACGTGATGGTATCATGCCAGAAAGCAGCGGGGGGCCCGAAGCCGCCGCTTTT
GTTAAAGTGTCAATGGACGGGGCTCCATACCTGAGGAAGATCGATCTCCGGATGTACA
AGTCTTACGATGAACTGAGCAACGCGCTTTCAAACATGTTCTCATCTTTCACCATGGGA
AAGCATGGGGGCGAAGAAGGAATGATTGACTTCATGAATGAGAGAAACTGATGGATC
TCGTCAATTCTTGGGACTACGTGCCTTCATACGAGGATAAGGATGGAGATTGGATGCTG
GTAGGAGACGTGCCTTGGCCCATGTTCGTGGACACTTGCAAAAGGCTCAGACTGATGA

AGGGTAGCGATGCCATCGGCTTGGCACCCCGCGCGATGGAGAAGTGTAAATCTAGGG
CC

Table S1: oligonucleotides used for qRT-PCR, STAR METHODS

Amplicon	Forward	Reverse
PIGV US	AAGGGGTTGTTGGGAAGTGA	CCACTTGACCATGCTTGCAT
PIGV DS	AGTTCAGGGCTTCACAGTGA	CTCAGGCCTCTAAACCCCAA
PCF11 US	TGACCATTCTAGCCGAGGAG	GGGGTTGGAGAGAAGGAACA
PCF11 DS	CACACTGGCTCTGCACAAAT	CACACGAACATGCAGGAAGT
PIGV SPL	GACCCTAGAGAAGCCCGATC	CTCAACAGCGGCTCTTGATC
PCF11 SPL	TGAAGAAGAGGAGGAATGGCA	GGGTTCCTGCAATTCGTTTT
GAPDH SPL	GCACCACCAACTGCTTAGC	ATGATGTTCTGGAGAGCCCC
ACTB SPL	CATCCGCAAAGACCTGTACG	CCTGCTTGCTGATCCACATC
PPM1G	GCCTGGCCAAGTACTTCCTA	CCTCTTCCTTCGTTCCCAGT
STK11IP	GGGAGTCTAAGGAAAAGGAG	CAGTGAAAGGAGAGCGTATC
SERPINB8	ACCAAGCAAAGGAGTCAGGA	ACGTCCACCCAAACATTCTC
RBM39	GGAAATAGTGGAGAAAAGCA	CATTTTTGAAGGAACGGTAG
FOXP4-AS	TGCACAATTTCACACCTAGA	ATGTTAGTGACACCTGCACA
SEPHS1 PROMPT	TCTCCACATTTCACGAGGCT	ATTTGCACAGGAGGCTAGGA
DIS3 SPL	ACCCTCACTTAAAATAGAAGATACAGT	CCATTAAGGTCCATGTTTGAAGT
CLIP4 SPL	ATTTTCTGCTTCTGATACCCCA	CCCACTGTCTCAAAATGGCA
CLIP4 US	GTCAGGCTGTTCACGTCATC	TTTCAAAGGCGCCCGTTTTA
CLIP4 DS	TCCTTTGTTTGGAAGATACCCA	GGCGTAACAGAGAAGTCAAGT
SEPHS1 SPL	GGAAACATGTTCGGCCTCAT	CTATGATTCTGGCTGTGCGG
SEPHS1 US	TGAGCGCCTTCCTGATACAA	TTTAACACAGCCTCACCCCT
SEPHS1 DS	GGTGTCATGTGAACCTGCAG	CTGCCAGCGAATCAAGTGAA

QUANTIFICATION AND STATISTICAL ANALYSIS

qRT-PCR was quantitated using the comparative quantitation function associated with the Qiagen Rotorgene instrument. Values were first normalised to ACTB or GAPDH and then samples were compared by quantitating the experimental values relative to the control condition (given the value of 1 by the software). Bars show the average of at least three replicates and error bars show the standard deviation. Where assessed, p values were calculated using a student's t-test.

DATA AND SOFTWARE AVAILABILITY

All sequencing data, generated in this study, are deposited with Gene Expression Omnibus. We also analysed data deposited previously. Accession numbers are: XRN2-AID data

(GSE109003); DIS3-AID RNA-seq, EXOSC10-AID RNA-seq and EXOSC10^{CAT} iCLIP (GSE120574); EXOSC10^{WT} iCLIP (GSM1892061 & GSM1892062); H3K27ac ChIP-seq (GEO: GSE31755); H3K4me1 ChIP-seq (GEO: GSE31755), H3K4me3 ChIP-seq (GEO: GSE35583); ChIP input control (GEO: GSE31755).
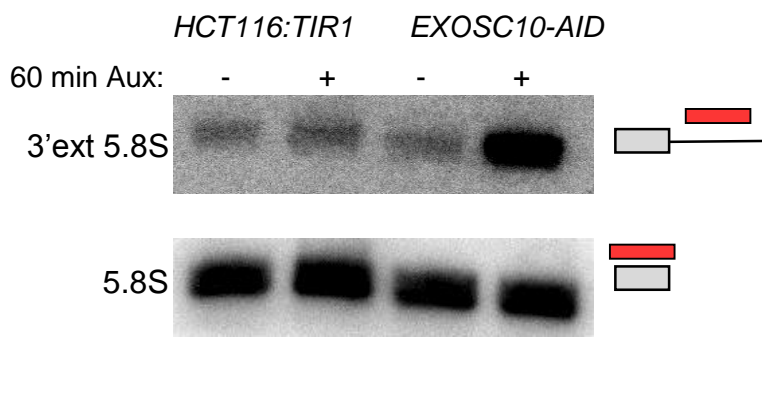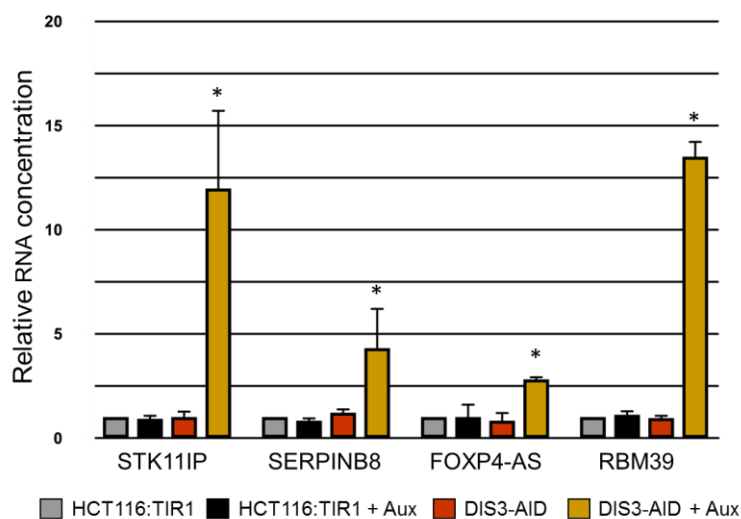
Figure 1

A

Homology Directed Repair

Allele 1:

Allele 2:

B

Davidson et al_ Figure 1

HCT116:TIR1   *EXOSC10-AID*

Aux (mins):   0   60   0   15   30   60

EXOSC10-AID

EXOSC10

Protein Remaining (%):   100   35   9   3

C

HCT116:TIR1   DIS3-AID

Aux (60mins)   -   +   -   +

α-DIS3   DIS3-AID
                               DIS3

α-Tubulin

DIS3 mRNA: 1   1.2   0.46   0.53
qRT-PCR   +/-0.22 +/-0.14 +/-0.18

D

HCT116:TIR1   DIS3-AID

Aux (60mins)   -   +   -   +

Dis3-AID
(α-AID)

α-Tubulin

E

GFP-MTR4:   +   -   +   -   +   -   +   -

α-GFP

α-EXOSC2

5% Input   IP

F

Aux: -   +   -   +   -   +

α-EXOSC10

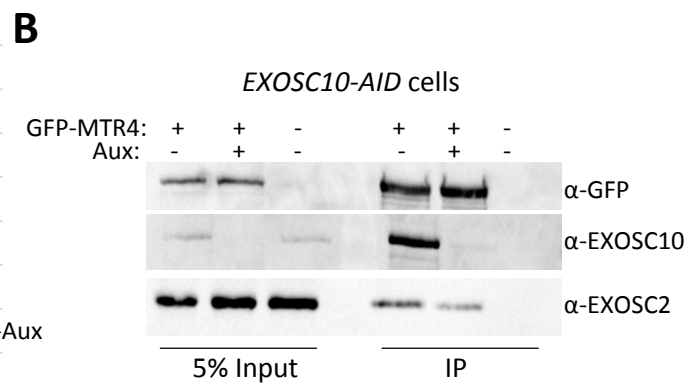α-DIS3

α-MTR4

α-EXOSC2

α-EXOSC3

α-CPSF73

Figure 2

Davidson et al_ Figure 2

A

B

C

D

Figure 3

A

MARS2

EXOSC10 -Aux [0-2318]
EXOSC10 +Aux [0-2318]
DIS3 -Aux [0-2318]
DIS3 +Aux [0-2318]

PPM1G

EXOSC10 -Aux [0-3352]
EXOSC10 +Aux [0-3352]
DIS3 -Aux [0-3352]
DIS3 +Aux [0-3352]

SEPHS1

EXOSC10 -Aux [0-2419]
EXOSC10 +Aux [0-2419]
DIS3 -Aux [0-2419]
DIS3 +Aux [0-2419]

6 kb

B

N=4701

EXOSC10-AID Minus Aux
EXOSC10-AID Plus Aux
DIS3-AID Minus Aux
DIS3-AID Plus Aux

Average read density

Distance to feature (kb)

C

Antisense   Sense

8:8,290,610

EXOSC10-AID -Aux [0-5799]
EXOSC10-AID +Aux [0-5799]
DIS3-AID -Aux [0-5799]
DIS3-AID +Aux [0-5799]

10 kb

X:45,705,862

EXOSC10-AID -Aux [0-4712]
EXOSC10-AID +Aux [0-4712]
DIS3-AID -Aux [0-4712]
DIS3-AID +Aux [0-4712]

17 kb

D

N=960

EXOSC10-AID Minus Aux
EXOSC10-AID Plus Aux
DIS3-AID Minus Aux
DIS3-AID Plus Aux

Average read density

Distance to eRNA transcript (bp)

E

PCF11

EXOSC10 -Aux [0-7203]
EXOSC10 +Aux [0-7203]
DIS3 -Aux [0-7203]
DIS3 +Aux [0-7203]

PIGV

EXOSC10 -Aux [0-6251]
EXOSC10 +Aux [0-6251]
DIS3 -Aux [0-6251]
DIS3 +Aux [0-6251]

7 kb

F

N=4356
EXOSC10-AID Minus Aux
EXOSC10-AID Plus Aux
DIS3-AID Minus Aux
DIS3-AID Plus Aux

Intron 1

Average read density

Scaled intron (5 kb)

Figure 4

Davidson et al_ Figure 4

Figure 5

Davidson et al_ Figure 5

A

B

C

D

EXOSC10-AID -Aux   EXOSC10-AID +Aux   DIS3-AID - Aux   DIS3-AID +Aux

Figure 6

A

XRN2-AID −Aux
XRN2-AID +Aux

MYC PROMPT

RBM39 PROMPT

B

XRN2-AID −Aux
XRN2-AID +Aux

N=3293

C

CLIP4

EXOSC10-AID -Aux
EXOSC10-AID +Aux
DIS3-AID -Aux
DIS3-AID +Aux

26kb

SEPHS1

EXOSC10-AID -Aux
EXOSC10-AID +Aux
DIS3-AID -Aux
DIS3-AID +Aux

13kb

D

US   DS

PCF11

XRN2-AID -Aux   XRN2-AID +Aux

E

Spliced RNA

XRN2-AID -Aux   XRN2-AID +Aux

F

Proxy of attenuated transcription frequency

DIS3-AID -Aux   DIS3-AID +Aux

A

8:8,290,610 | X:45,705,862

EXOSC10-AID -Aux [0-5799] | [0-4712]
EXOSC10-AID +Aux [0-5799] | [0-4712]
DIS3-AID -Aux [0-5799] | [0-4712]
DIS3-AID +Aux [0-5799] | [0-4712]
H3K27ac [0-347.9] | [0-368.3]
Log2 H3K4me1/ H3K4me3 [-3.89-5.27] | [0-4.97]

10 kb | 17 kb

Antisense | Sense

B

MARS2 | *SEPHS1*

EXOSC10-AID -Aux [0-2318] | [0-2420]
EXOSC10-AID +Aux [0-2318] | [0-2420]
DIS3-AID -Aux [0-2318] | [0-2420]
DIS3-AID +Aux [0-2318] | [0-2420]
H3K27ac [0-40.4] | [0-217]
Log2 H3K4me1/ H3K4me3 [-8.27-2.98] | [-8.58-2.88]

6 kb | 6 kb

Antisense | Sense

C

Intron 1 reads normalised to exon 1

DIS3-AID Minus Aux R1
DIS3-AID Plus Aux R1
DIS3-AID Minus Aux R2
DIS3-AID Plus Aux R2

Average read density

Distance from First Exon 5' ss (kb)

D

Intron 2:

N=3905

EXOSC10-AID Minus Aux
EXOSC10-AID Plus Aux
DIS3-AID Minus Aux
DIS3-AID Plus Aux

Average read density

5' End   Scaled intron (5 kb)   3' End

E

Intron 4:

N=3200

EXOSC10-AID Minus Aux
EXOSC10-AID Plus Aux
DIS3-AID Minus Aux
DIS3-AID Plus Aux

Average read density

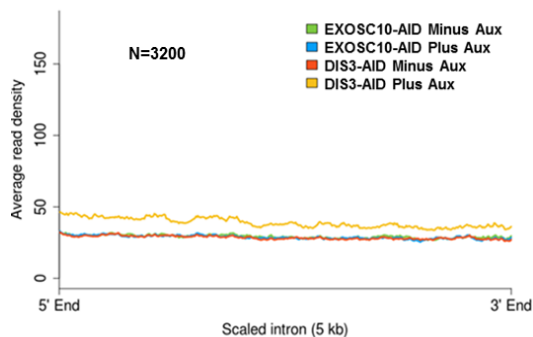5' End   Scaled intron (5 kb)   3' End

Figure S1: Further analysis of eRNA regions and pre-mRNA stability in *EXOSC10-AID* and *DIS3-AID* cells, related to Figure 3

(A) Examples of eRNA stabilised upon DIS3 loss. These regions show bi-directional transcription (red and blue are signals from opposite strands) and a high level of H3K4me1 versus H3K4me3 characteristic of eRNA transcription. Y-axis shows RPKM for RNA-seq. Lower panel of each figure shows H3K4me1 (blue) vs H3K4me3 (red). H3K4me1 density shown above the line with H3K4me3 below.

(B) Two protein-coding genes shown for comparison with part A. In this case, promoter regions are associated with low H3K4me1 but higher levels of H3K4me3. Scales are as for A. Both eRNA and protein-coding promoters show H3K27ac modification.

(C) Metagene showing enhanced reads over the first intron of genes upon auxin treatment of *DIS3-AID* cell lines. Unlike main text Figure 3F, this representation shows the intron reads normalised to read density in the upstream first exon which was also higher in auxin treated samples possibly because of the general stabilisation of truncated RNAs. For auxin treated DIS3-AID samples, read-density was therefore normalised to the average difference in exonic read-density compared to untreated samples. Finally, both exon and intron metagene profiles were merged into a single profile demarcated by a dotted line. R1 and R2 corresponds to different biological replicates of each experiment.

(D) Metagene showing RNA-seq reads across the second intron of genes in *EXOSC10-AID* and *DIS3-AID* cells treated or not with auxin. The effect of DIS3 loss is diminished relative to the first introns. The plot is not normalised to exon 1 and generated as for Figure 3F.

(E) As for A, but for intron 4. Note, that the effect of DIS3 loss is near absent by this stage in transcription. The plot is not normalised to exon 1 and generated as for Figure 3F.
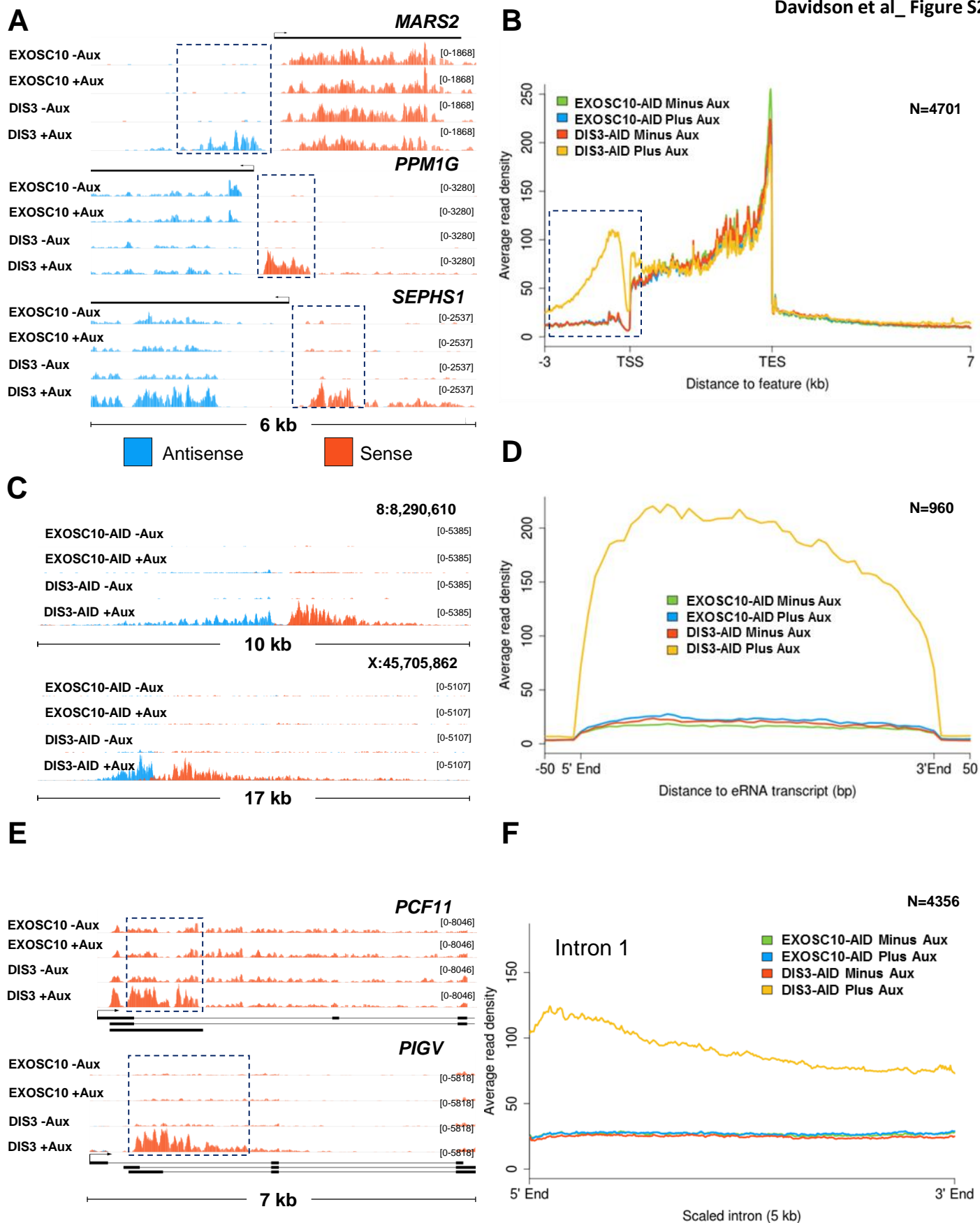
Figure S2: Biological replicate of *DIS3-AID* and *EXOSC10-AID* RNA-seq, related to Figure 3
This figure is the same as main text figure 3 except the data are derived from a second biological repeat of the RNA-seq.
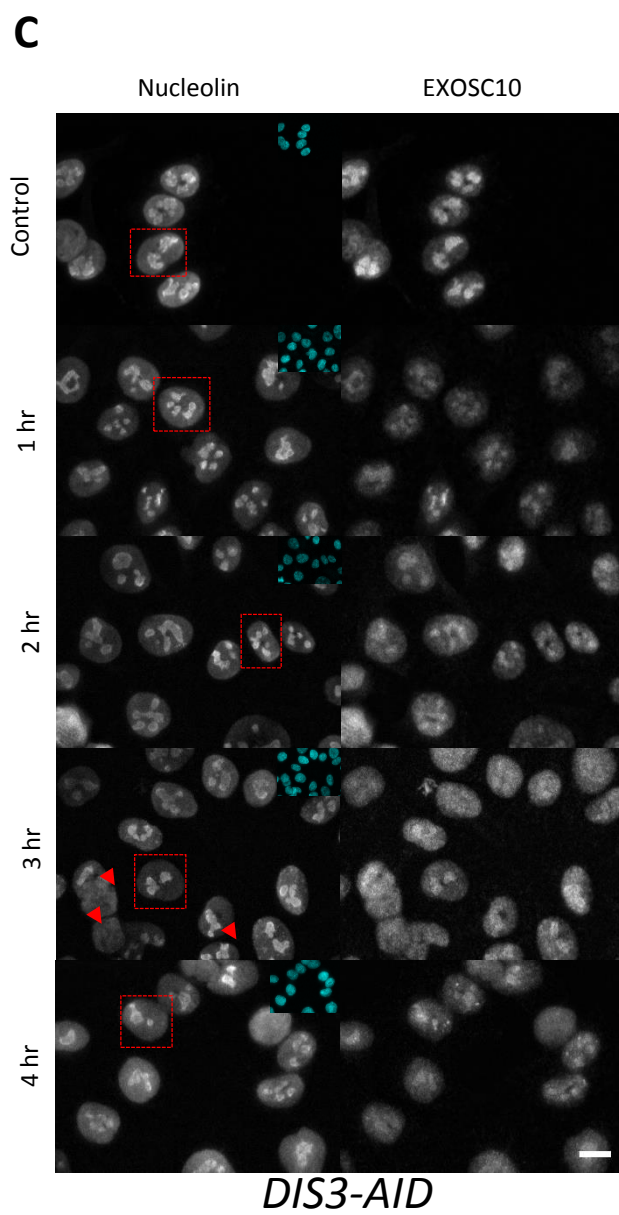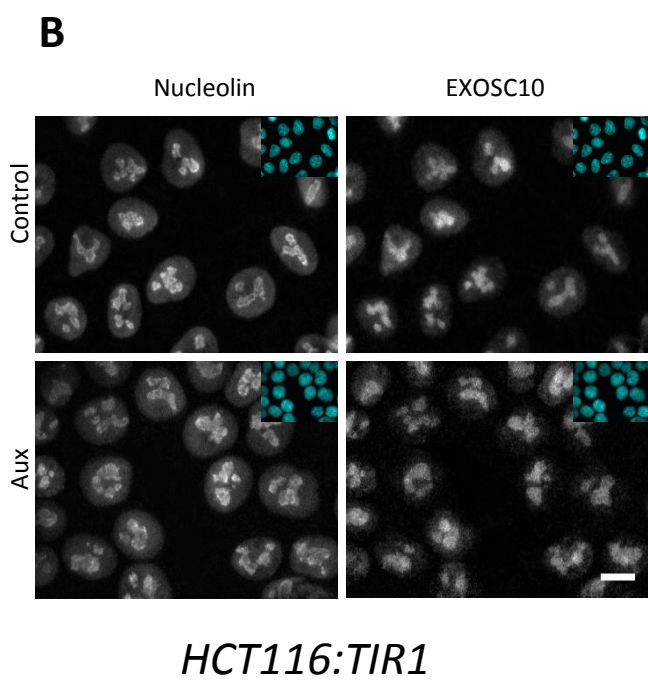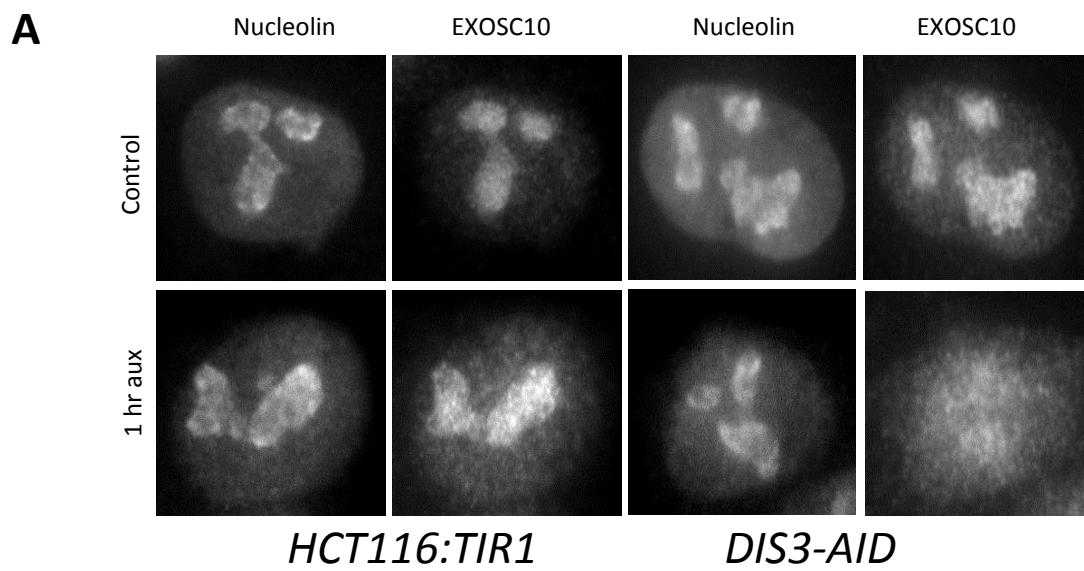Accordingly, annotations are the same as for main-text figure 3.

A

HCT116:TIR1   *DIS3-AID*

B

HCT116:TIR1

C

DIS3-AID

Figure S3: Analysis of EXOSC10 localisation in *HCT116:TIR1* and *DIS3-AID* cells treated or not with auxin, related to Figure 4F)

(A) Immunofluorescence experiment whereby *HCT116:TIR1* or *DIS3-AID* cells grown in the presence or absence of auxin (1 hr) are stained for EXOSC10 or nucleolin. This representation is an enlarged view (of a different cell for DIS3-AID to highlight generality) compared to Figure 4F used to further illustrate that DIS3 loss affects EXOSC10 staining in the nucleoli of *DIS3-AID* cells. In contrast, auxin treatment of parental (*HCT116:TIR1*) cells does not impact on EXOSC10 nucleolar staining.

(B) Immunofluorescence experiment whereby *HCT116:TIR1* cells grown in the presence or absence of auxin are stained for EXOSC10 or nucleolin. This experiment confirms the nucleolar location of EXOSC10 and that auxin treatment does not affect this.

(C) A wider field of *DIS3-AID* cells representing the conditions shown in Figure 4F. In each field, the individual cell used in Figure 4F is boxed. Note that 24.6% of cells contain EXOSC10 puncta at the 4h time point (based on a random count of 191 cells, within 13 fields of view across replicates).
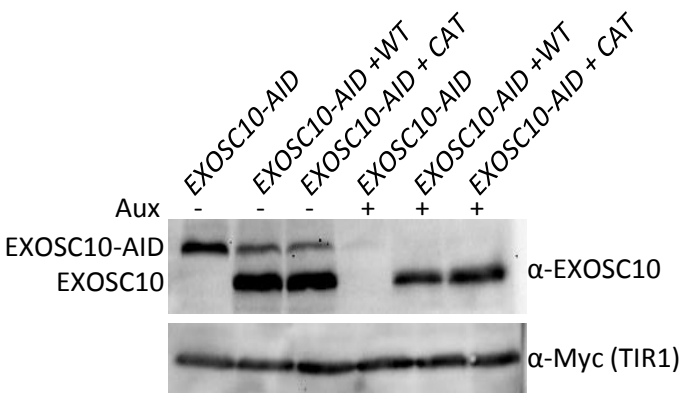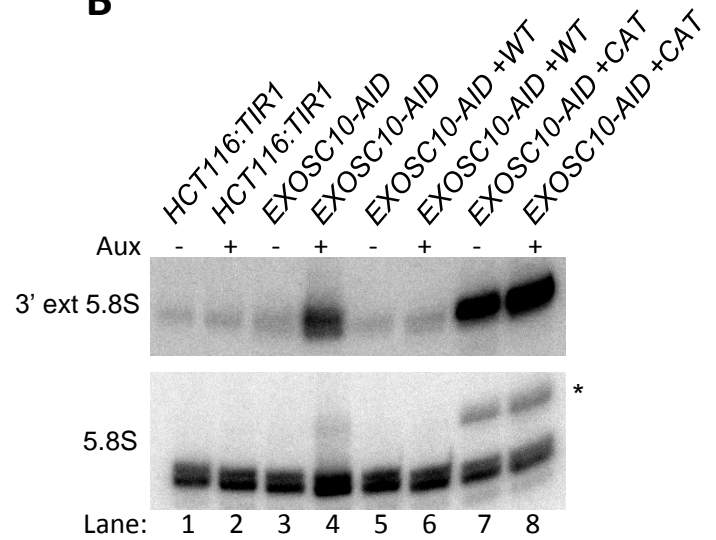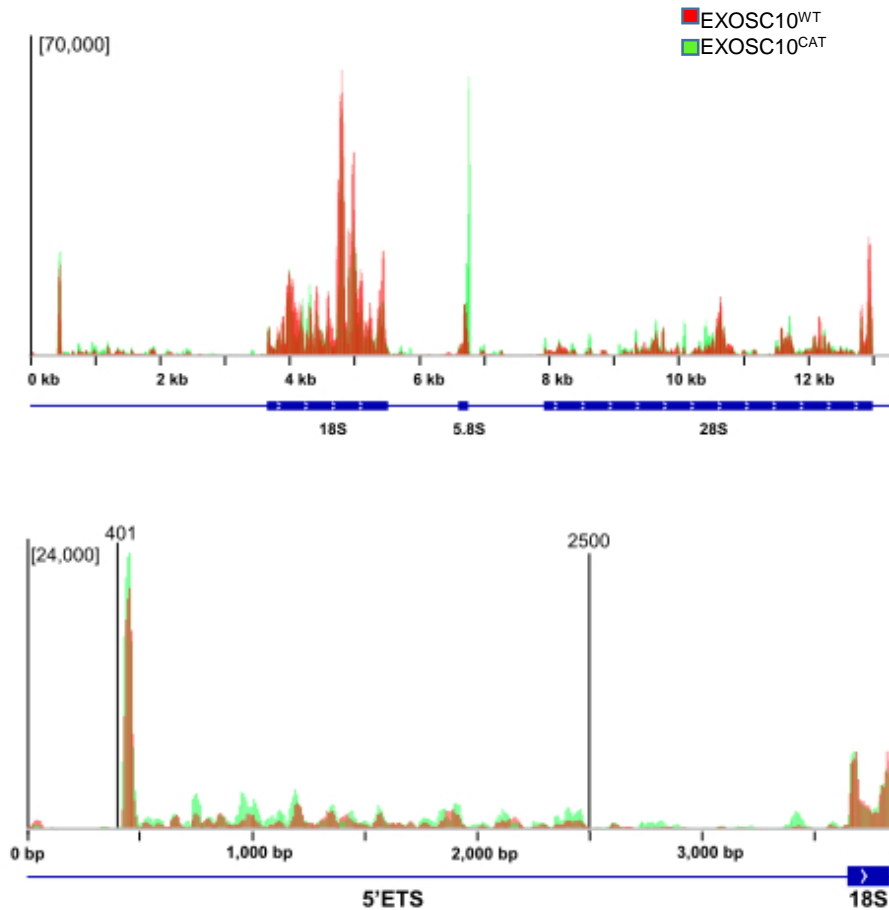
A

	EXOSC10-AID	EXOSC10-AID +WT	EXOSC10-AID + CAT	EXOSC10-AID	EXOSC10-AID +WT	EXOSC10-AID + CAT
Aux	-	-	-	+	+	+

EXOSC10-AID
EXOSC10

α-EXOSC10

α-Myc (TIR1)

B

	HCT116:TIR1	HCT116:TIR1	EXOSC10-AID	EXOSC10-AID	EXOSC10-AID +WT	EXOSC10-AID +WT	EXOSC10-AID +CAT	EXOSC10-AID +CAT
Aux	-	+	-	+	-	+	-	+

3' ext 5.8S

5.8S   *

Lane: 1   2   3   4   5   6   7   8

C

EXOSC10^{WT}
EXOSC10^{CAT}

[70,000]

0 kb   2 kb   4 kb   6 kb   8 kb   10 kb   12 kb

18S   5.8S   28S

[24,000]   401   2500

0 bp   1,000 bp   2,000 bp   3,000 bp

5'ETS   18S

Figure S4: Inactive EXOSC10 causes dominant negative stabilisation of rRNA precursors, related to Figure 5

(A) Western blotting of EXOSC10 in *EXOSC10-AID* cells or *EXOSC10-AID* cells stably expressing either wild-type (WT) or inactive EXOSC10 (CAT). In each case, samples show cells treated or not with auxin (1h). This demonstrates the selective depletion of only the AID tagged version.

(B) Northern blotting of the same cell lines and conditions in (A) whereby mature 5.8S rRNA (lower panel) or the 3' extended version (upper panel) were detected. The 3' extended version is also detected by the mature probe (*). Note that expression of inactive EXOSC10 has a dominant negative effect on the accumulation of the 3' extended form, consistent with our iCLIP whereas expressing the WT protein has no such effect (compare lanes 1, 5 and 7).

(C) iCLIP track of 45S rRNA locus showing iCLIP read density obtained from EXOSC10^{WT} or EXOSC10^{CAT}. iCLIP reads are obtained across the whole locus but there is a striking accumulation of reads 3' of the 5.8S gene in the EXOSC10^{CAT} sample. Units are reads per million mapped. Lower track is zoomed to the 5'ETS sequence making it clear that there are sites of EXOSC10 binding, some of which are modestly enhanced in EXOSC10^{CAT} samples. Units are reads per million mapped.

A

	SNORD	SNORA	SCARNA	Total
WT	87 (68%)	61(56%)	10(66%)	158(63%)
CAT	122(96%)	95(88%)	10(66%)	227(91%)
Bound snoRNA	127	108	15	250

B

EXOSC10-AID -Aux   EXOSC10-AID +Aux   DIS3-AID - Aux   DIS3-AID +Aux
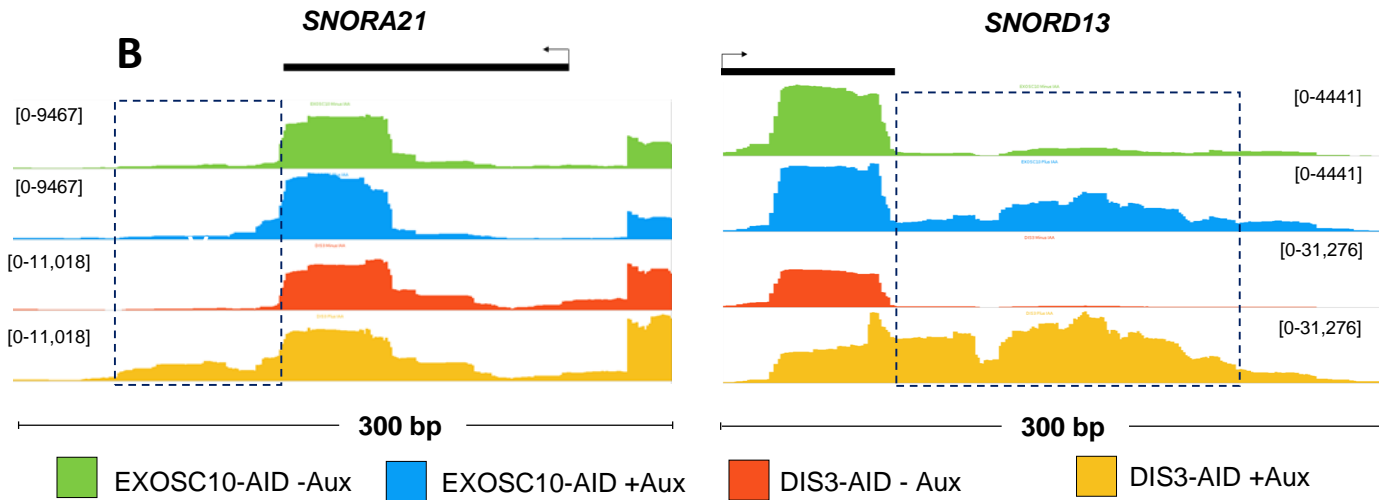
C

	WT %	CAT %	CAT/WT
Total	100	100	1
PROMPT	0.11210626	0.1022381	0.91197516
eRNAs	0.22840467	0.2552155	1.11738286
5' flank snoRNA	0.06893386	0.08152661	1.18267877
Mature snoRNA	3.77523574	2.79753413	0.74102237
3' flank snoRNA	0.14452782	0.30087676	2.08179129

D
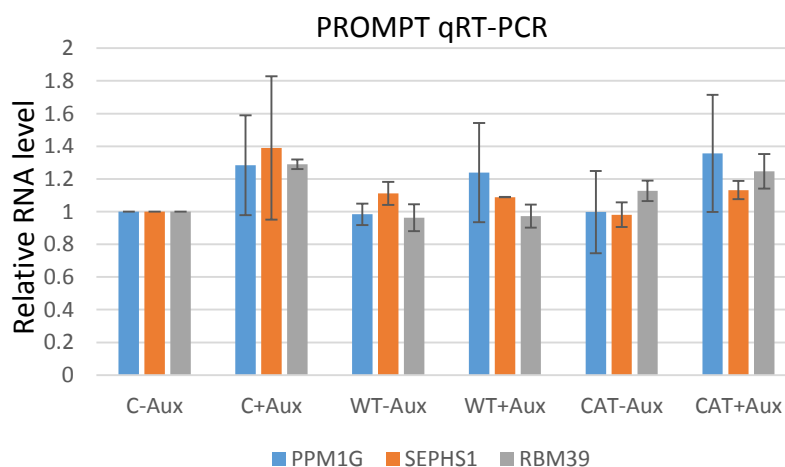
Figure S5: Analysis of snoRNA 3' extensions upon EXOSC10 or DIS3 loss, related to Figure 5

(A) Table summarising the percentage of expressed snoRNAs bound by either EXOSC10^{WT} or EXOSC10^{CAT}.

(B) IGV track of SNORA21 and SNORD13 in *EXOSC10-AID* and *DIS3-AID* cells treated or not with auxin. SNORA21 shows a longer 3' extension when DIS3 is depleted and a shorter one when EXOSC10 is lost. SNORD13 also shows extended stabilisation upon loss of DIS3 and, more mildly, EXOSC10. SNORD13 was the only example we found showing longer extensions in both cell lines.

(C) Table showing the proportion of iCLIP reads in the WT and CAT experiment that correspond to PROMPT, eRNA, 5' flank of snoRNA, mature snoRNA or 3' flank of snoRNA. Also shown is the uplift (or not) in the proportion of reads as a result of using the inactive EXOSC10 (CAT/WT). *Bone fide* substrates, exemplified by 3' extended snoRNAs (red box), are more enriched in the CAT experiment. However, PROMPTs and eRNAs are not enriched in this manner arguing that they are not normally EXOSC10 substrates – an observation supported by our RNA analyses.

(D) qRT-PCR analysis of PPM1G, SEPHS1 and RBM39 PROMPTs in *EXOSC10-AID, EXOSC10-AID+WT* or *EXOSC10-AID+D313A* cells treated or not with auxin (1h). Values are shown relative to those obtained in untreated *EXOSC10-AID* cells after normalising to GAPDH levels. Error bars are standard deviation.
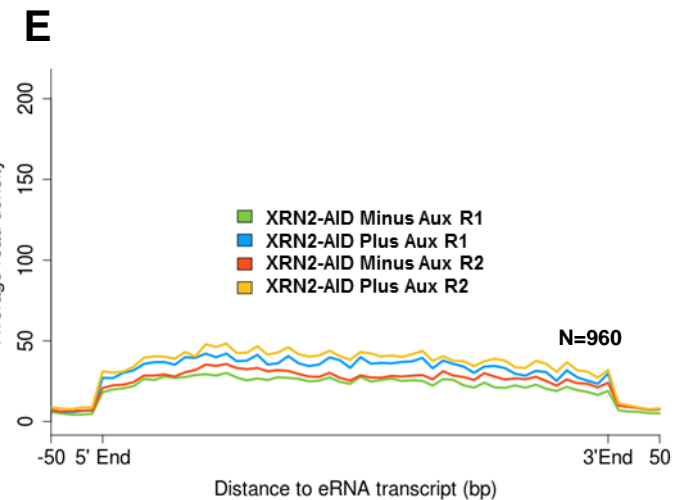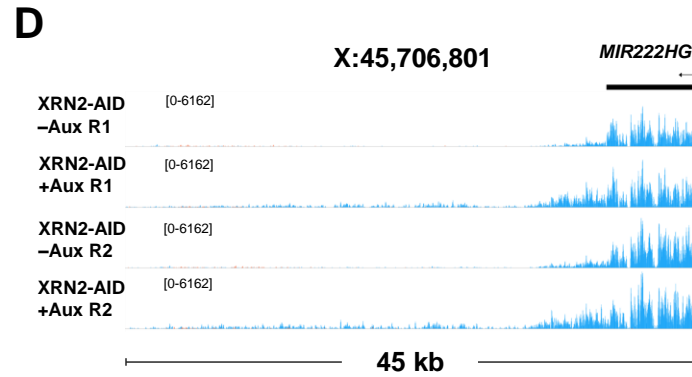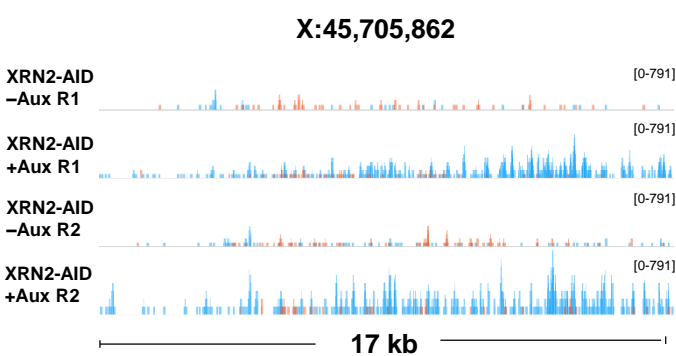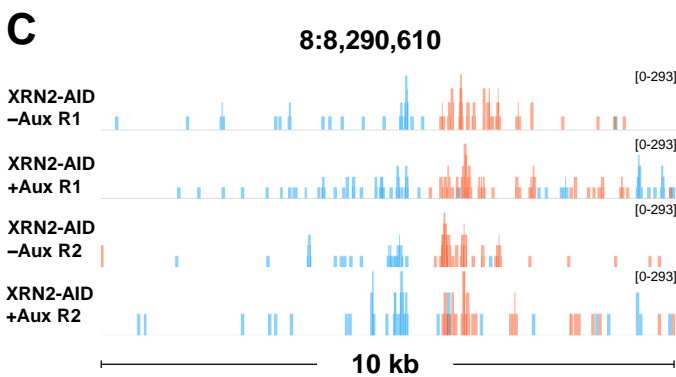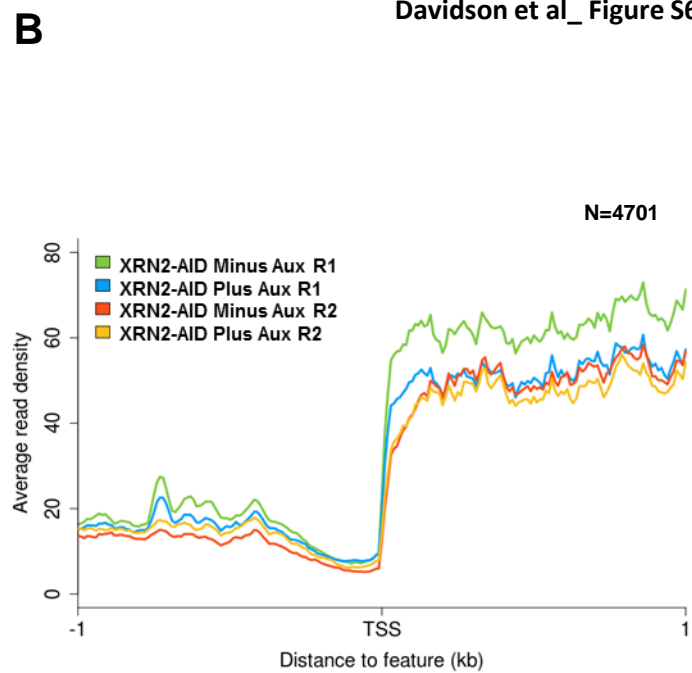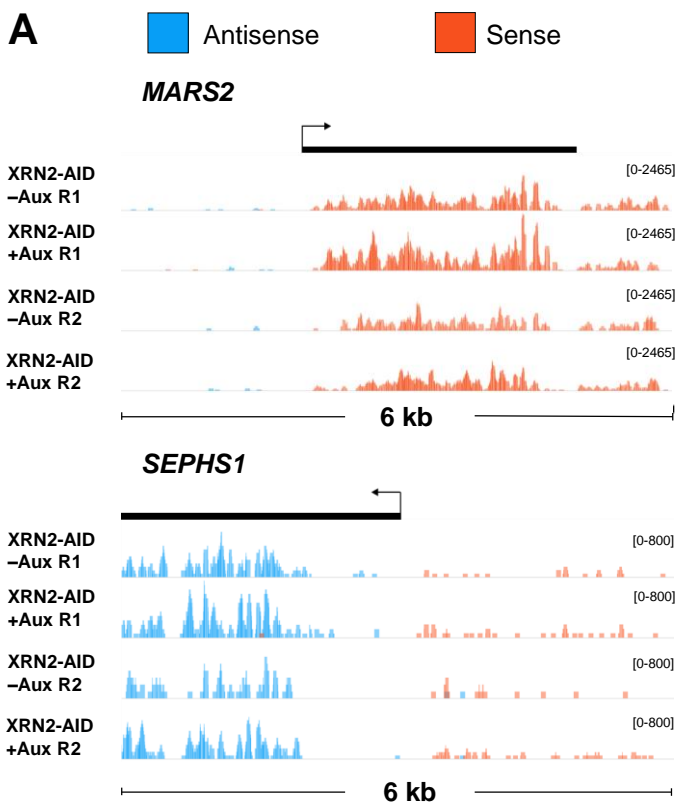
Figure S6: XRN2 plays no role in degrading PROMPT, eRNA or attenuated pre-mRNA, related to Figure 6

(A) *MARS2* and *SEPHS1* PROMPT regions in RNA-seq data obtained from *XRN2-AID* cells treated or not with auxin. Note that there is a lack of XRN2 effect on PROMPT region RNAs (boxed) in both cases. "R1" and "R2" denotes two biological replicates. Y-axis units are RPKM.

(B) Metaplot of promoter regions in RNA-seq data obtained from *XRN2-AID* cells treated or not with auxin. Note that there is a general lack of XRN2 effect on PROMPT region RNAs consistent with our mNET-seq analyses in Figure 6.

(C) Tracks showing the same eRNA regions represented in Figure 3C in RNA-seq data obtained from *XRN2-AID* cells treated or not with auxin. 8:8,290,610 shows no XRN2 effect. Whilst there is an enhanced anti-sense XRN2 effect for X:45,705,862 this is due to a termination defect on a nearby micro RNA expressing gene and not due to eRNA expression (part D of this figure). Note, that we have previously demonstrated that genes with 3' microRNAs are subject to XRN2-mediated termination (Eaton et al., 2018).

(D) IGV track of *MIR222HG* showing read-through transcription into the X:45,705,862 eRNA region (boxed) when XRN2 is lost. This, not any role of XRN2 in eRNA stability, is responsible for the apparent increase in anti-sense signal seen in part C of this figure. It is also consistent with our previous findings (Eaton et al., 2018) that XRN2 terminates transcription following miRNA processing.

(D) Metaplot of eRNAs in RNA-seq data obtained from *XRN2-AID* cells treated or not with auxin. Note that there is a general lack of XRN2 effect on eRNAs.